ERS-2 Wind Scatterometer Cyclic Report

from 8th May 2000 to 12nd June 2000
Cycle 53

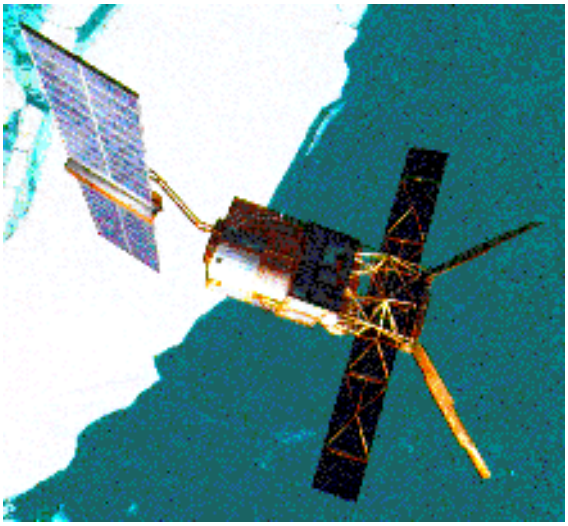

Prepared by:	PCS team	ESRIN APP-ADQ
Inputs from:	F. Aidt	ESTEC TOS-EMS
	L. Isaksen	ECMWF

Document No: APP-ADQ/PCS/WS00-006
Issue: 1.0
Date: 3th, July 2000

Distribution List

ESAHQ	G. Duchossois	
ESTEC	M. Canela	APP-LR
	E. Attema	SCI-VRS
	F. Aidt	TOS-EMS
	B. Gelsthorpe	APP-LTP
	R. Zobl	
	K. van't Klooster	
ESOC	F. Bosquillon de Frescheville	TOS-OFC
	L. Stefanov	TOS-OFC
ESRIN	M. Albani	APP-AD
	P. Lecomte	APP-ADQ
	V. Beruti	APP-ADF
	S. Jutz	APP-ADU
	G. Kohlhammer	APP-AM
	M. Onnestam	APP-ADC
	U.Gebelein	Serco

L.A. Breivik	DNMI
P. Snoeij	DUT
J. Heidbreder	DORNIER
L. Isaksen	ECMWF
J. Kerkman, J. Figa	EUMETSAT
S. Pouliquen	F-PAF
V. Wismann	IFARS
A. Cavanie	IFREMER
R.S. Dunbar	JPL
A. Stoffelen, T. Driessenaar	KNMI
G. Legg, P. Chang	NOAA/NESDIS
W. Gemmill	NOAA/NWS
J. Hawkins	NRL
D. Offiler, R. Graham, C.A. Parrette	UK-MET Office
F. Courtier, H. Roquet	Meteo-France
C. Scupniewicz	FNMOC
R.A. Brown	University of Washington
J. Boutin	LODYC/UPMC

This report and its annex are also available via FTP.
ftp pooh.esrin.esa.it (login as anonymous)
cd pub/SCATTEROMETER
wscatt_rep_53.ps.Z, annex_rep_53.ps.Z

1.0 Introduction and summary

The document includes a summary of the daily quality control made within the PCS and various sections describing the results of the investigations and studies of "open-problems" related to the scatterometer, e.g. the CMOD-4 for high wind speed, the antenna pattern. In each section results are shown from the beginning of the mission in order to allow comparisons and to outline possible "seasonal" effects. An explanation for the major events which have impacted the performance since launch is given, and comments about the recent events which occurred during the last cycle are included.

This report covers the period from 8th May 2000 to 12nd June 2000 (cycle 53).

Calibration performance

- The monitoring of the interbeam calibration confirms that the differences between the signals measured with the various beams during the ascending passes has a seasonal behaviour. On average differences are close to 0.1 dB during the summer and are increasing to 0.2 dB during the winter. For the descending passes, the differences between the winter and the summer are less clear and the inter-beam calibration stays around 0.1 dB.
- This monitoring confirms also the evolution of the signal difference (aft-fore) and (aft-mid) during descending passes. During the last cycles the difference (aft-fore) is slightly closer to 0. dB. Investigations have been carried out and more details are included in section 2.3.3. To summarise these results it can be noted that this evolution has mainly affected the aft antenna with a mean decrease of roughly 0.05 dB. No clear correlation has been found between the antenna temperature and these differences in the gamma nought. It is not easy to estimate if this evolution started at the end of year 1999 or at the beginning of year 2000. Because of the noise present in these time series, it is also difficult to estimate if this evolution of the aft antenna signal during the descending passes, is related to the instrument or to mission events. The most relevant mission events during this period are: the payloads switch-off to face out the Leonid meteorite shower (November 1999), a series of AMI emergency switch down anomalies and the AOCS mono-gyro configuration (February 2000).
- The position of the gamma nought histograms maxima computed over the rain forest is stable within 0.5 dB. These 0.5 dB are related to the geophysical noise present in the time series. Therefore the small deviation in the aft signal at descending passes detected by comparison among the signals of the three antennae (0.05 dB) is not visible by this type of analysis.
- The evolution of the sigma nought computed per relative track and for each node across the swath is stable. Four tracks over the rain forest has been selected to monitor the sigma nought (two for the ascending passes and two for the descending ones). The relative tracks used to monitor the time series (since December 1997 onwards) show a good correlation among the nodes (near and far range) and the stability of the sigma nought ranges from 0.2 to 0.5 dB depending on the node and on the track. The time series for descending tracks is more stable than the ones computed for ascending passes.
- For cycle 53 the antenna patterns over the Brazilian rain forest (large area) are not available from ESTEC due to an hardware problem. The antenna patterns, computed by PCS over a small area of the Brazilian rain forest for the cycle 53, are very close to the ones obtained in the previous cycle. The antenna patterns show a flat profile, within 0.5 dB for the descending passes (with a small slope at near range) and within 0.4dB for the ascending ones.

- The antenna temperature monitoring over the Brazilian rain forest confirms the increase of roughly 1 degree per year for the mid and fore antenna and roughly 2 degrees per year for the aft antenna. The increase in the antennae temperature could be related with the degradation, during the years, of the antennae protection film.
- During the cycle 53 the transponders were working nominal only for two calibration passes and no results of the calibration exercise are available yet.

Instrument performance

- The internal calibration level shows that the power decrease during the cycle 53 was 0.1 dB. The power decrease estimation over a larger period is regular and is not affected by the AMI anomalies. Since 26th October 1998 (cycle 37) the power decrease is, on average, 0.08 dB per cycle and the total power decrease from cycle 37 to cycle 53 is on average 1.3 dB.
- The daily averaged CoG of the received spectrum shows stable results. The large variation of the doppler frequency on 30th May 2000 is related to the fact that the satellite was in FPM. The analysis of the evolution of the doppler frequency as function of the ascending node time shows that the doppler frequency (roughly after 5200 s. from the ascending node) was more stable compared with the previous cycle. There is a good agreement between the Doppler frequency and the reference sinusoidal pattern. The main difference between the two is around 4500 s. after the ascending node.
- The noise power level evolution is stable.

Product performance

- The AMI instrument has been operated in wind and wind/wave mode 90.7% of the ascending passes total operation time and 84.7% of the descending passes total operation time. AMI unavailability, descoping and data lost are excluded. These values are within the nominal range.
- PCS quality control has reported stable results for cycle 53. The number of valid triplets acquired per day was stable around 180000. The wind speed bias (UWI -ECMWF Forecast) was close to 0.1 m/s and the wind speed standard deviation was between 2.5 m/s and 3.0 m/s. The ambiguity removal rate was working fine for more than 90% of nodes and the wind direction is accurate for the 93% of the nodes. The bad performance (high wind speed bias and low percentage of ambiguity removal rate) in the geophysical validation on 30th May 2000 is due to the spacecraft attitude. On that day the satellite was in FPM which is less accurate than the nominal one YSM.
- The ECMWF reports (cycle 53) an average wind speed bias of -0.78 m/s (UWI) and of -0.51 m/s (4D-Var). The wind directional bias is close to zero (both UWI and 4D-Var products) and the direction standard deviations were ranging between 30 and 65 degrees (UWI) and between 15 and 30 degrees (4D-Var). These results are comparable to the results from the previous cycle.

The report is available via ftp (login as anonymous) to the address pooh.esrin.esa.it directory / pub/SCATTEROMETER file names: wscatt_rep_53.ps.Z, annex_rep_53.ps.Z (Unix compressed) and on the PCS web site: http://pcswww.esrin.esa.it (Scatterometer performance page). The statistics about the availability of the ERS-2 Wind Scatterometer raw data during cycle 53 and the detailed list of the unavailability periods are given in the document “ERS-2 AMI/RA/ATSR/GOME availability statistics” issued at the end of each cycle. Post processed Scatterometer data acquired

over tropical cyclones are available on the web site: http://pcswww.esrin.esa.it (cyclone tracking page).

2.0 Calibration Performances

The calibration performances are estimated using three types of target: a man made target (the transponder) and two natural targets (the rain forest and the ocean). This approach allow us to design the correct calibration using a punctual but accurate information from transponders and an extended but noisy information from rain forest and ocean for which the main component of the variance comes from the geophysical evolution of the natural target and from the backscattering models used. These aspects are in the calibration performance monitoring philosophy. The major goals of the calibration monitoring activities are the achievement of a “flat” antenna pattern profile and the assurance of a stable absolute calibration level.

2.1 Gain Constant over transponder

One gain constant is computed per transponder per beam from the actual and simulated two-dimensional echo power, which is given as a function of the orbit time and range time. This parameter clearly indicates the difference between “real instrument” and the mathematic model. In order to acquire data over the transponder the Scatterometer must be set into an appropriate operational mode that is defined as “Calibration”.

Table 1 shows the result of the calibration plan for cycle 53. The “Yes” in the EWIC column means that the raw data are available, “No” means the opposite case. The “On” in the transponder status column means that, from the raw data (EWIC), the transponders has been recognised as switched-on; “Off” means the opposite case. The “Yes” in the GC computed column means that a gain constant value has been retrieved, “No” means the opposite case.

As reported in the table no new gain constants have been computed by ESTEC.

TABLE 1. Calibration Plan: Cycle 53

DATE	ORBIT (absolute)	ORBIT (relative)	Passage	Ground Station	EWIC (raw data)	AMI mode	Transponder Status	GC computed
000509	26415	8	D	KS	Yes	Calibration	Off	n/a
000512	26458	51	D	KS	Yes	Calibration	Off	n/a
000527	26680	273	A	MS	Yes	Calibration	On	No
000530	26723	316	A	MS	Yes	Calibration	On	No

Figure 1 and Figure 2 show the gain constants available since the beginning of the mission, the analysis is split for the different antenna elevation angle. From these figure it is clear that the gain constant measurements are stable (within +/-0.5 dB) but after the end of the commissioning phase (cycle 11) only few data are available.

The plots in Figure 3 show the value of the Gain Constant for the three beams and for the ascending, descending and all passes. The plots show the average of all gain constant available since January 1996 (cycle 8) for each antenna elevation angle. The antenna patterns are flat but there is a clear shift of the level of the curves. On average, the mid beam is 0.3 dB higher than the aft one

and 0.5 dB higher than the fore one. For the descending passes the antenna pattern shows a slight negative slope from far range to near range.

Since September 1996 ESTEC has added a scaling factor to the gain constant in order to remove the bias among the three antennae. The gain constants were increased by 0.2 dB, -0.3 dB and 0.2 dB, for the fore, mid and aft beam respectively. The result is shown in Figure 4. The suggestion given by ESTEC has not been introduced into the ground processing because the antenna patterns computed over the rain forest do not show such bias (see Figure 5). So in the actual scenario, the differences among the antennae are considered as a bias due to the transponder themselves.

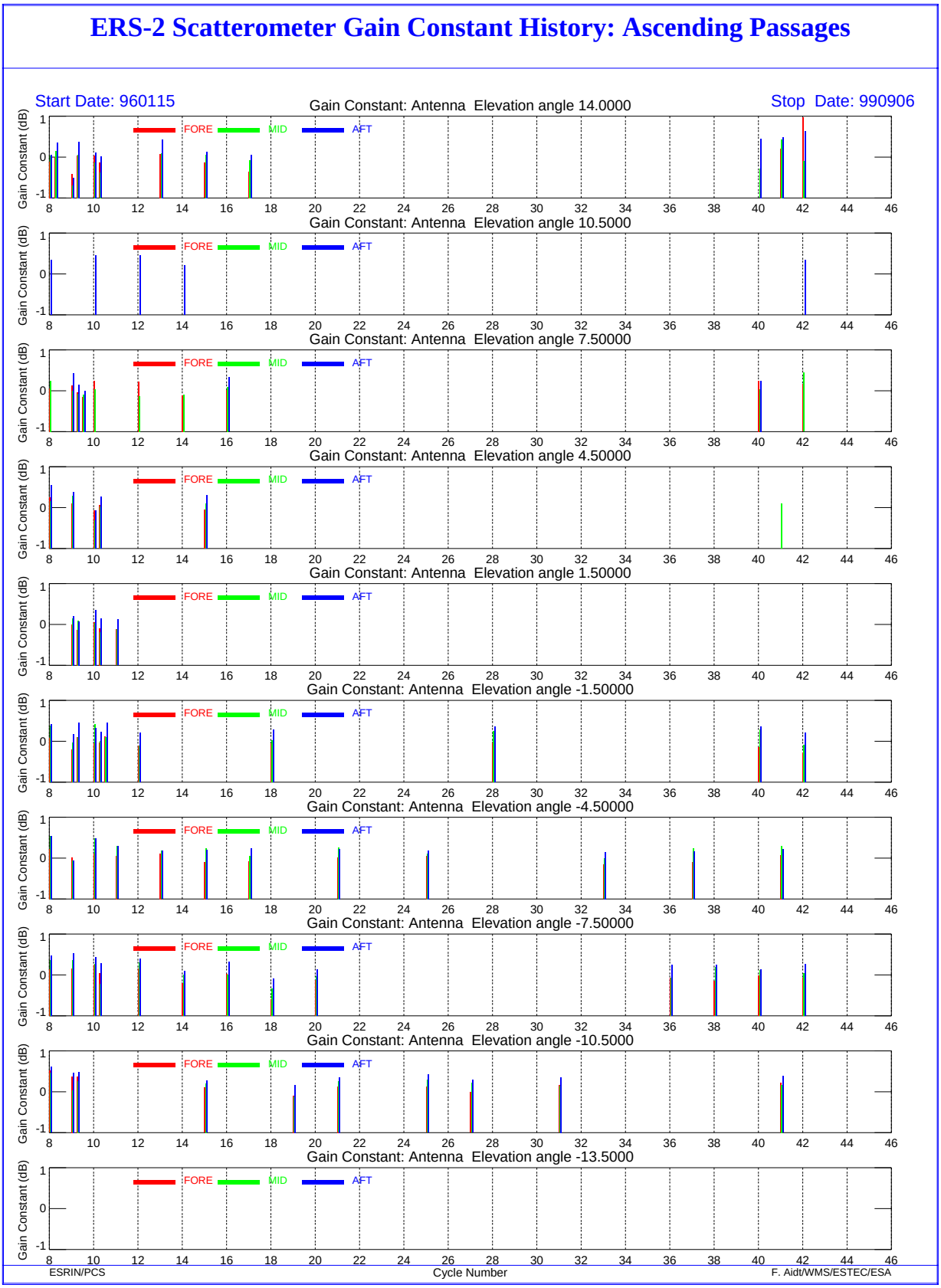

FIGURE 1. ERS-2 Scatterometer; gain Constant over transponder since the beginning of the mission (ascending passes).

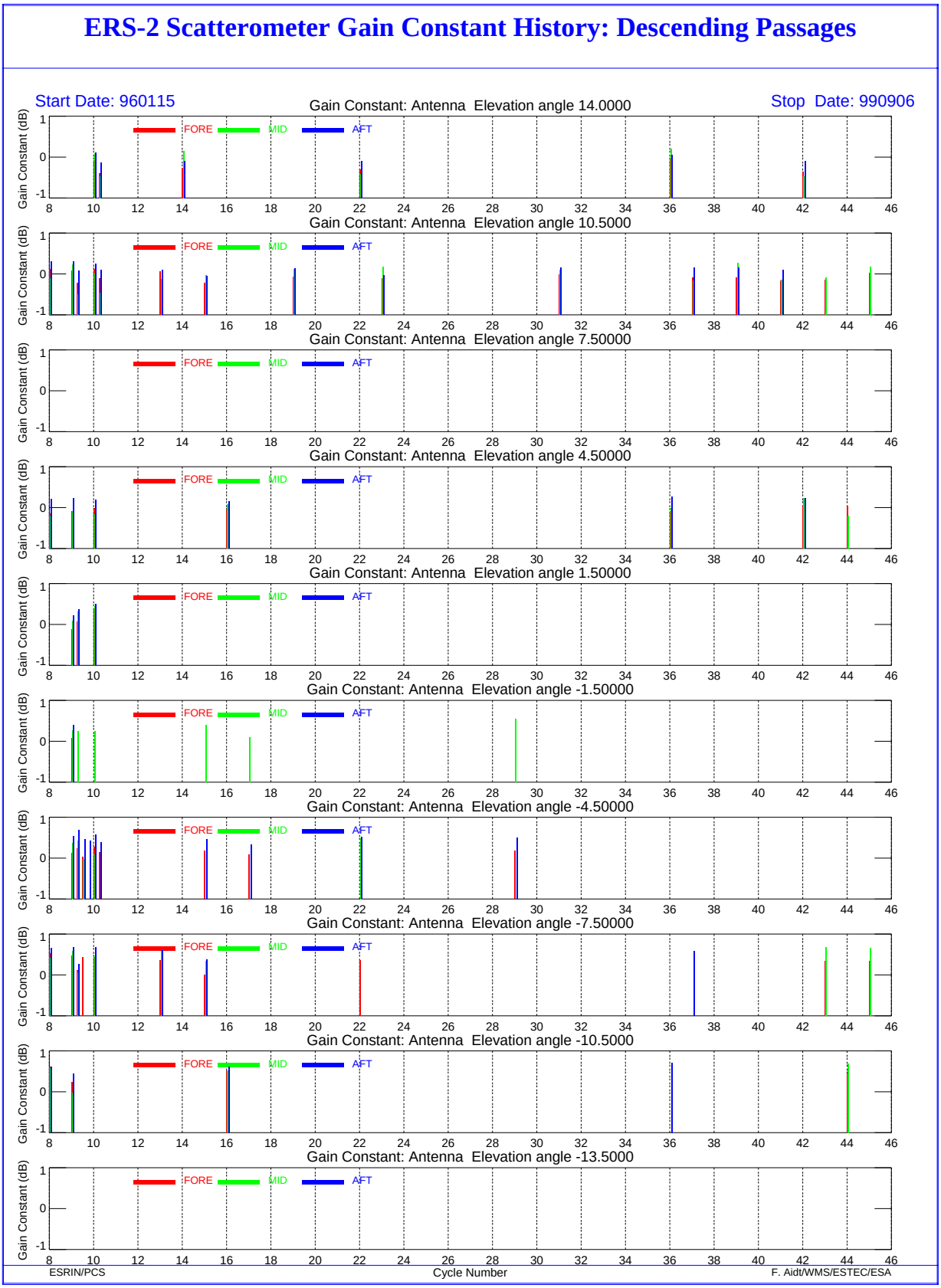

FIGURE 2. Scatterometer; gain Constant over transponder since the beginning of the mission (descending passes)

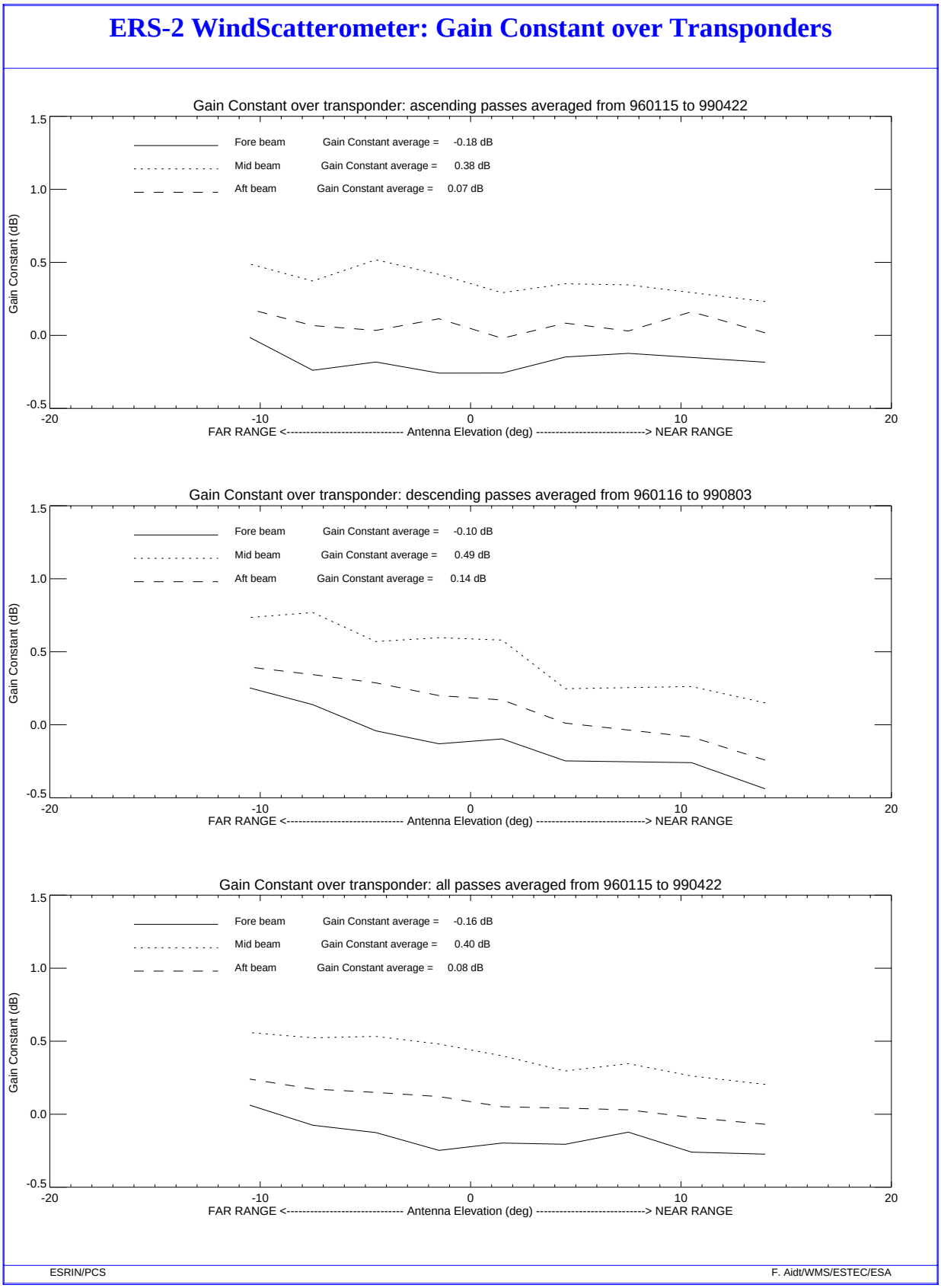

FIGURE 3. ERS-2 Scatterometer: gain constant over transponders. All data available since January 1996. Upper plot: ascending passes. Middle plot: descending passes. Lower plot: all passes.

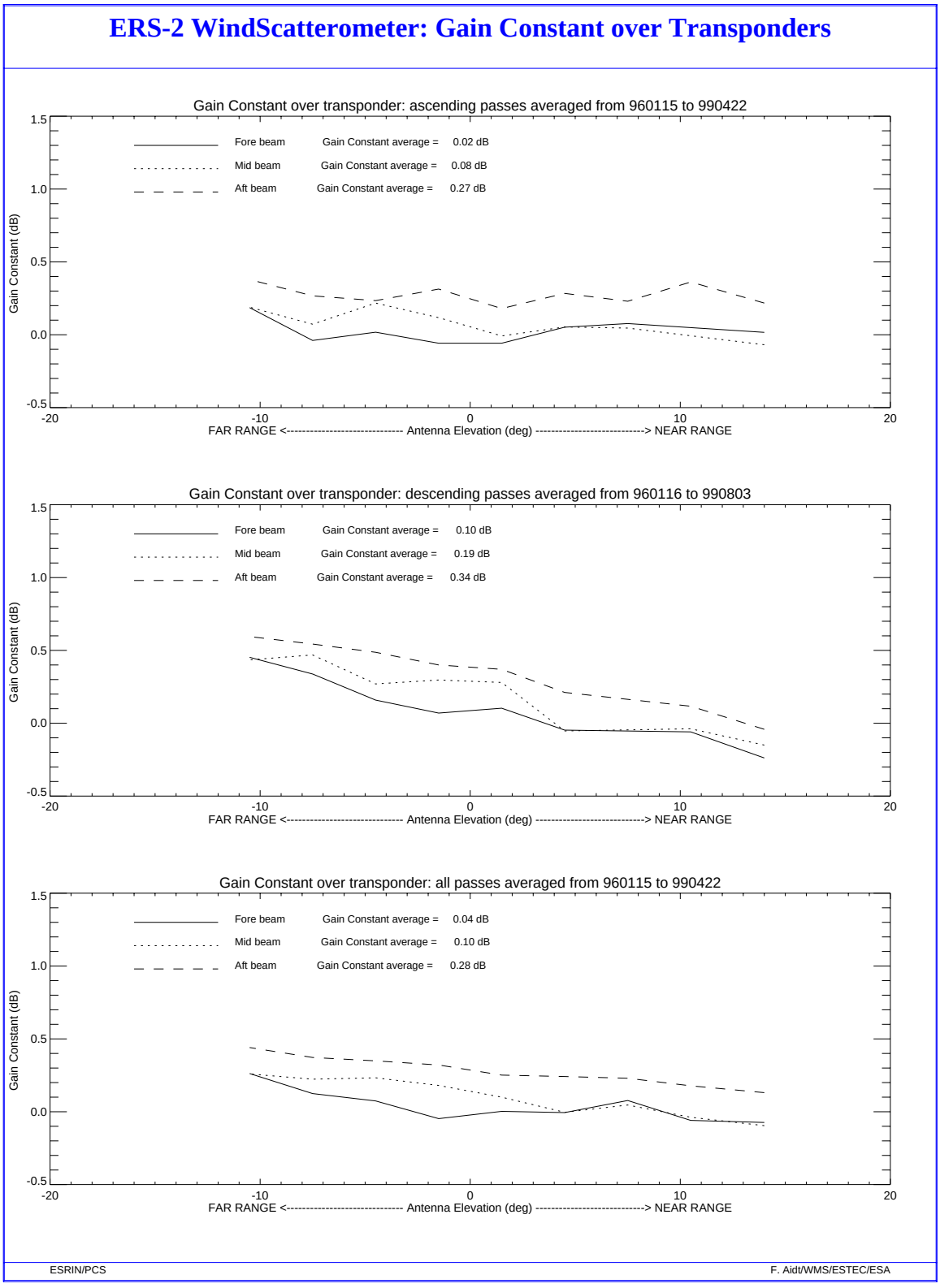

FIGURE 4. ERS-2 Scatterometer: gain constant over transponders plus a scaling factor. All data available since January 1996. Upper plot: ascending passes. Middle plot: descending passes. Lower plot: all passes.

2.2 Ocean Calibration

ECMWF performs the monitoring of ERS-2 sigma noughts over ocean (see the report in Annex).

The Scatterometer sigma noughts are compared with the ECMWF model first guess winds. The analysis is done for each incidence angle both ascending and descending passes. The result of the analysis are the antenna pattern biases.

The result of the monitoring for ascending tracks is a systematic larger negative bias than in cycle 52 (0.1 dB) for all three beams. It cannot be attributed to model changes and seems too large just to be due to seasonal variation. For the descending tracks the fore beam biases are slightly larger (with reference to cycle 52) for incidence angles between 25 and 40 degrees.

2.3 Gamma-nought over Brazilian rain forest

Although the transponders give accurate measurements of the antenna attenuation at particular points of the antenna pattern, they are not adequate for fine tuning across all incidence angles, as there are simply not enough samples. The tropical rain forest in South America has been used as a reference distributed target. The target at the working frequency (C-band) of ERS-2 Scatterometer acts as a very rough surface, and the transmitted signal is equally scattered in all directions (the target is assumed to follow the isotropic approximation). Consequently, for the angle of incidence used by ERS-2 Scatterometer, the normalised backscattering coefficient (sigma-nought) will depend solely on the surface effectively seen by the instrument:

$$S^0 = S \bullet \cos\theta$$

With this hypothesis it is possible to define the following formula:

$$\gamma^0 = \frac{\sigma^0}{\cos\theta}$$

Using this relation, the gamma-nought backscattering coefficient over the rain forest is independent of the incident angle, allowing the measurements from each of the three beams to be compared.

The test area used by the PCS is located between 2.5 degrees North and 5.0 degrees South in latitude and 60.5 degrees West and 70.0 degrees West in longitude.

The following paragraphs give a description of the activities carried out with this natural target.

2.3.1 Antenna pattern: Gamma-nought as a function of elevation angle

This analysis is carried out by ESTEC that has selected a larger region than the one used as test area within PCS. In this case the selected rain forest extends from 2.0 degrees South to 11.0 degrees South in latitude and 56.0 degrees West to 80 degrees West in longitude. A large area is selected in order to have a larger amount of measurements.

For cycle 53 the antenna patterns as function of the elevation angle have not been computed by ESTEC.

2.3.2 Antenna pattern: Gamma-nought as a function of incident angle

Figure 5 shows the antenna patterns as a function of the incidence angle for cycle 53.

The antenna patterns for the cycle 53 are very close to the ones obtained in the previous cycle. The antenna patterns show a flat profile, within 0.5 dB for the descending passes (with a small slope at near range) and within 0.4dB for the ascending. The mean level of the mid antenna profile is roughly 0.1 dB less than the fore and aft ones (in particular for the descending passes).

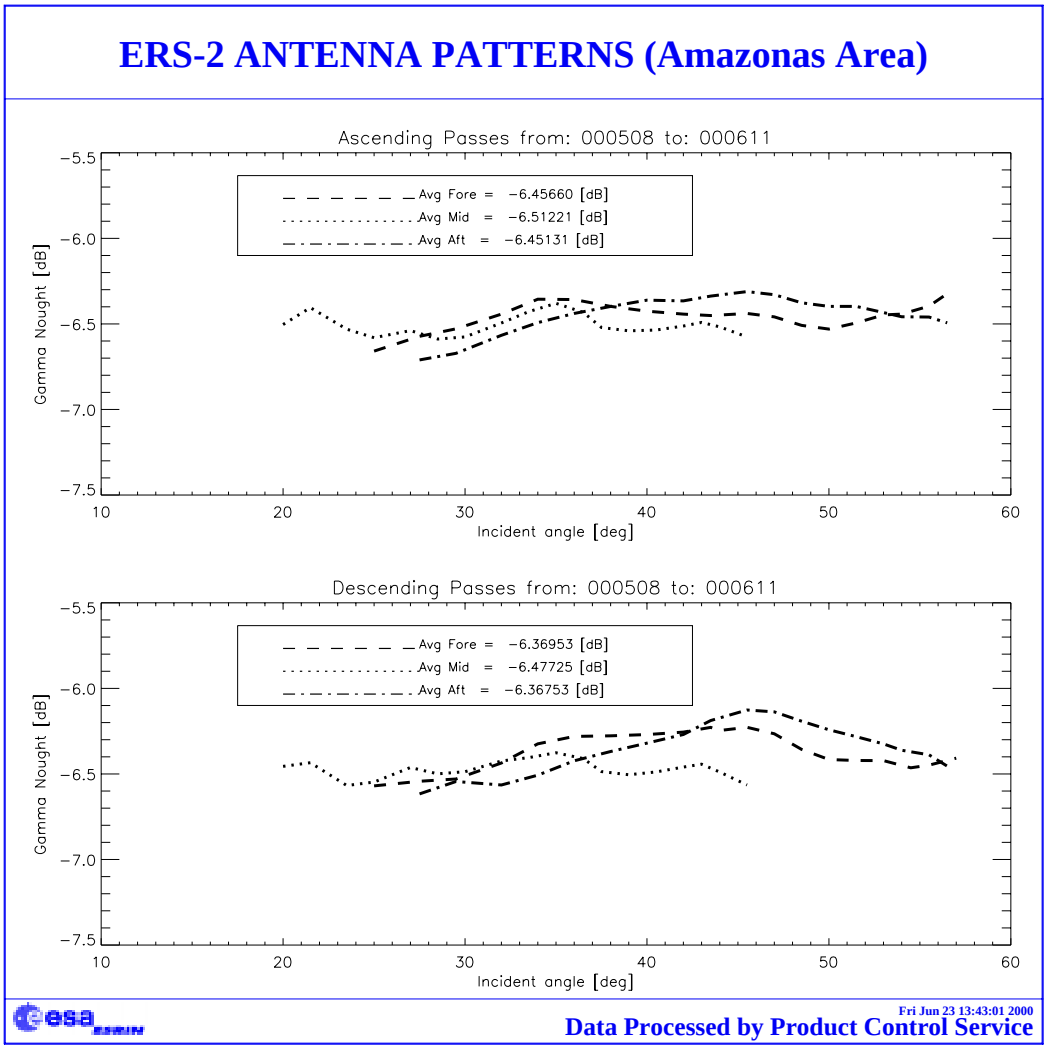

FIGURE 5. ERS-2 Scatterometer antenna patterns as function of the incidence angle: cycle 53.

2.3.3 Gamma-nought histograms and peak position evolution

As the gamma-nought is independent from the incidence angle, the histogram of gamma-noughts over the rain forest is characterised by a sharp peak. The time-series of the peak position gives some information on the stability of the calibration. This parameter is computed by fitting the histogram with a normal distribution added to a second order polynomial:

$$F\langle x\rangle = A_0 \cdot \exp\left(-\frac{z^2}{2}\right) + A_3 + A_4 \cdot x + A_5 \cdot x^2$$

where: $z = \dfrac{x - A_1}{A_2}$

The parameters are computed using a non linear least square method called “gradient expansion”. The position of the peak is given by the maximum of the function F(x). The histograms are computed weekly (from Monday to Sunday) for each antenna individually (“Fore”, “Mid”, and “Aft”) and for ascending and descending passage with a bin size of 0.02 dB.

Figure 6 shows the evolution of the histograms peak position since January 1996. The step shown in March 1996 is due to the end of commissioning phase when a new Look Up Table was used in the ground stations for WSCATT FD-products generation. It is interesting to note the decrease of roughly 0.2 dB from August 1996 to June 1997. This is linked to the switch of the Scatterometer calibration subsystem from side A to side B on 6th of August. The redundancy of side A device caused a little change in the calibration that was corrected on 19th June 1997 with a new calibration LUT used in the ground processing.

Figure 7 shows the evolution of the peak position corrected with the new calibration set also for the period from August 1996 to June 1997. From the plots in figure 7 it is clear that the calibration stability achieved over the rain forest is within 0.5 dB. A seasonal effect is also present in the peak position evolution for the three antennae.

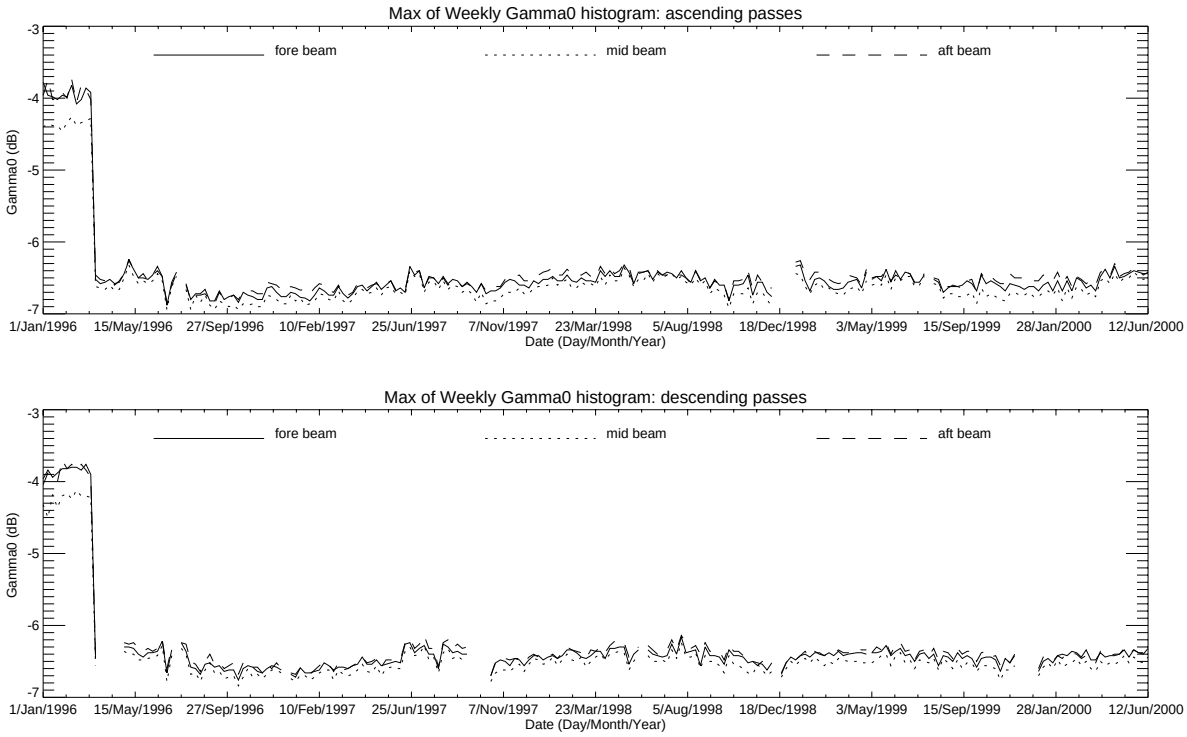

FIGURE 6. ERS-2 Scatterometer, gamma-nought histogram: weekly evolution of maximum position. From up to down: ascending passes, descending passes.

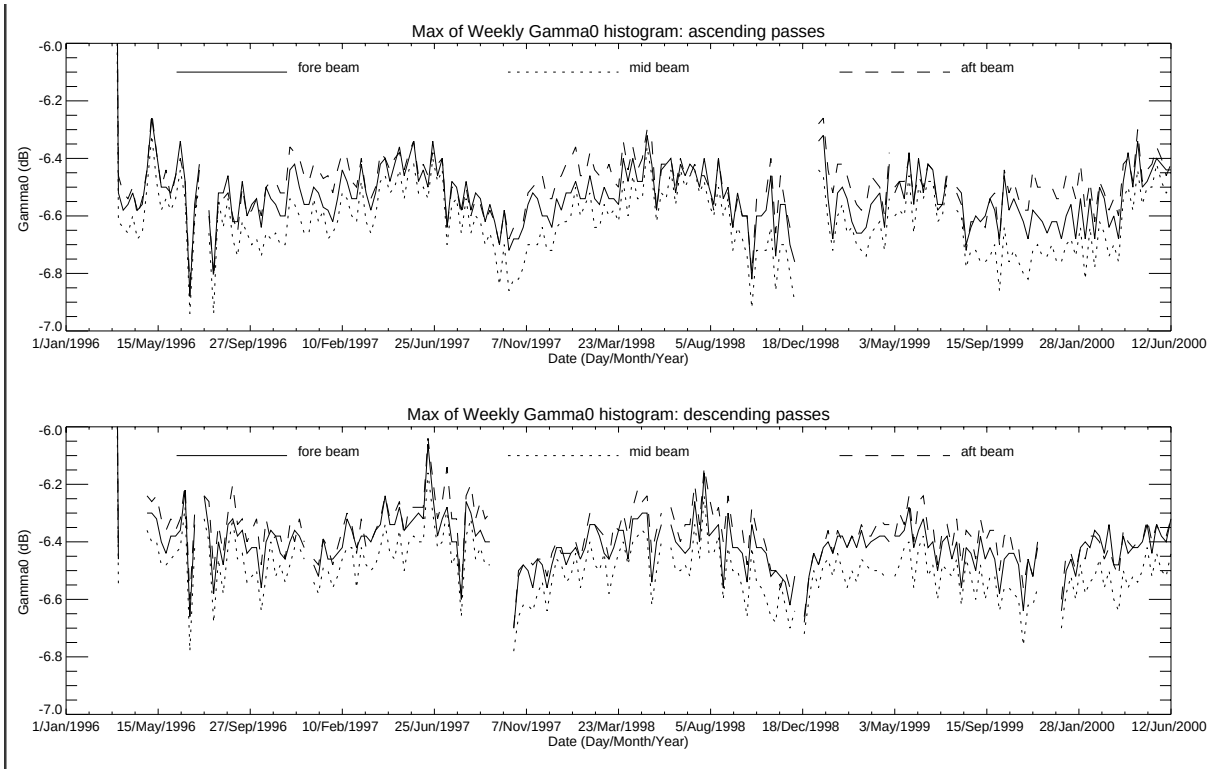

FIGURE 7. Gamma-nought histogram: weekly evolution of maximum position. Data from 6th of August 1996 to 19th June 1997 are corrected with the new calibration constant (+0.2dB). Upper plot: ascending passes. Lower plot: descending passes.

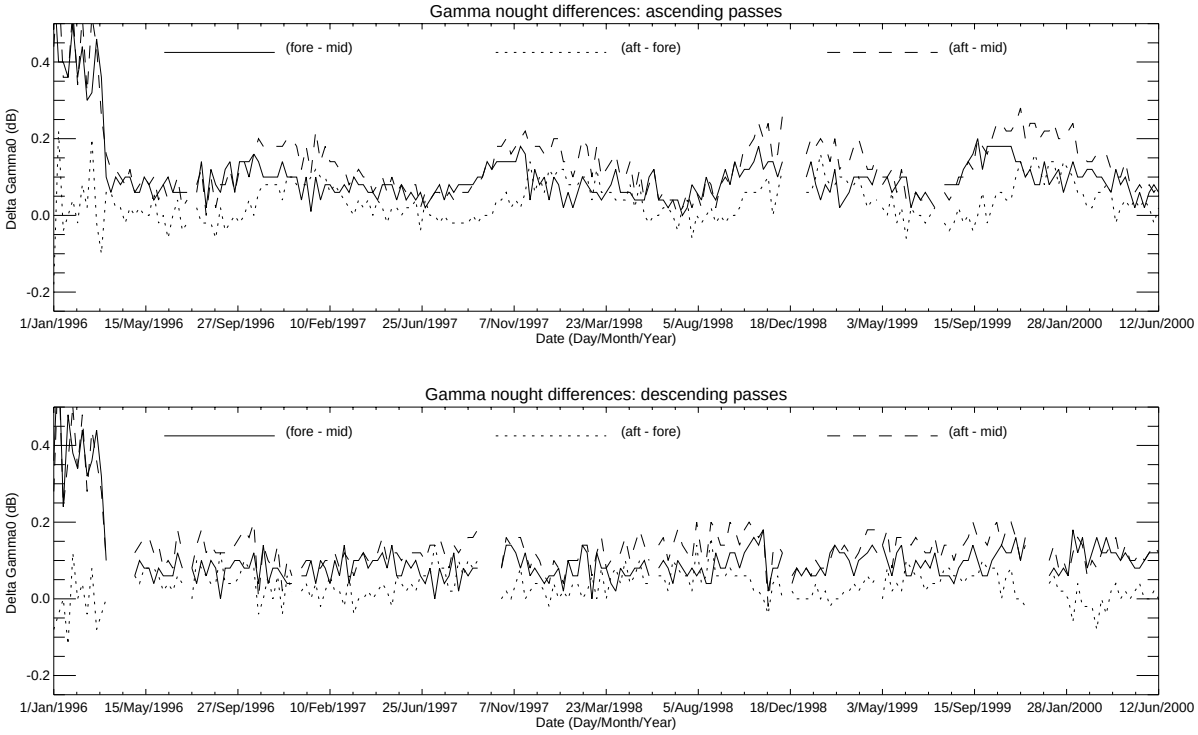

FIGURE 8. Inter-beam calibration, weekly differences of the maximum position since 1st January 1996. From up to down: ascending passes, descending passes.

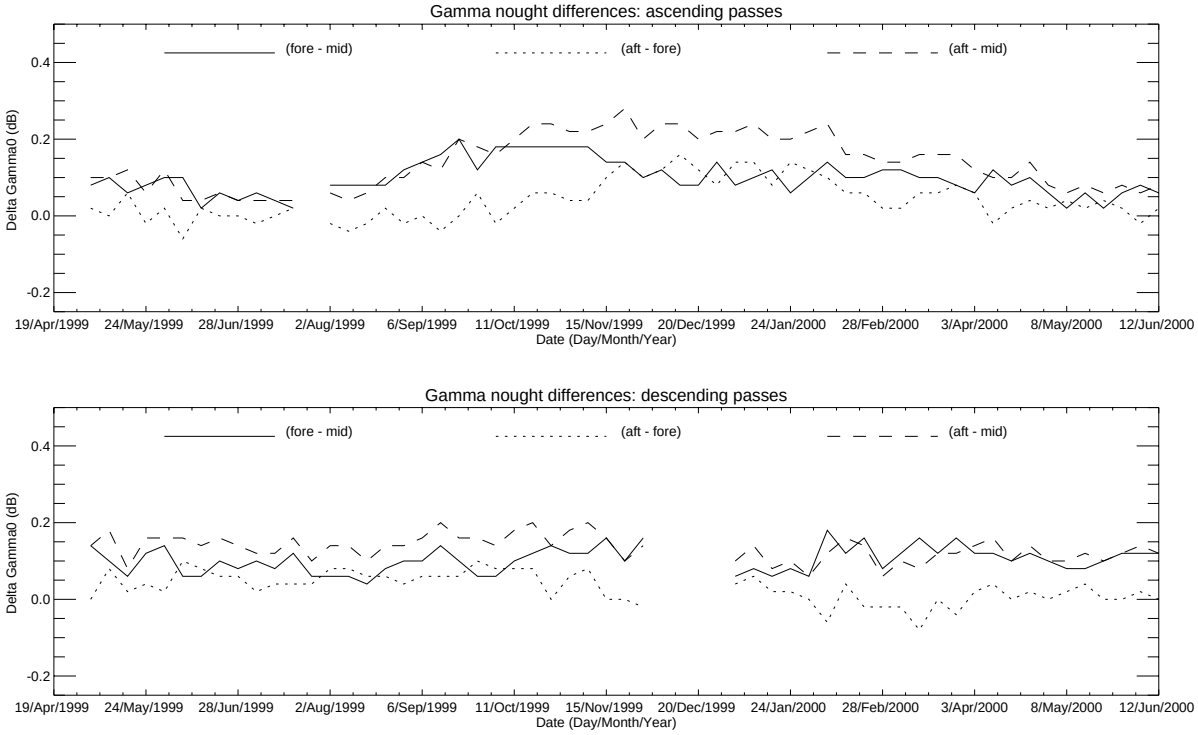

FIGURE 9. Interbeam calibration, weekly differences of the maximum position since cycle 42. From up to down: ascending passes, descending passes.

For the inter-beam calibration the results, since 1996 are shown in Figure 8.

For the ascending passes the differences in the signals have a seasonal behaviour. On average the differences are close to 0.1 dB during the summer and they are close to 0.2 dB during the winter. For the descending passes the differences between the winter and the summer are less clear and the inter-beam calibration is around 0.1 dB. A change around the end of year 1999 and the beginning of year 2000 is clear present in the (aft-fore) difference signal as well as in the (aft-mid) signal.

Figure 9 shows the inter-beam calibration during the last 11 cycles (from cycle 42 onwards). As reported in that figure the time series of the difference (aft-fore antenna), at descending passes, is now more close to 0. dB. It is not easy to judge if the change started in November 1999 or February 2000. The analysis of the plot (in Figure 9, bottom panel and dotted line) shows that values close to 0 dB was obtained in November 1999. During December 1999 only few data are available and a gap is present in the time series. On January 2000 the difference was moving from 0.05 dB to 0 dB and on February and March 2000 the difference was below 0. dB. From the beginning of April 2000 onwards the difference is stable around 0. dB. Consequently the difference (aft-mid) is more close to the difference (fore-mid) during the descending passes.

Investigations have been carried out in order to recognize which antenna has caused the change in the inter-beam calibration.

The Figures 10, 11 and 12 show the antenna patterns for the cycles 43, 52 and 42 respectively. With a delta cycle of 10 (350 days) is possible to compare the antennae profiles (and their averaged values) during the same season. This allows, in theory, to remove any geophysical signal. From the values reported in the figures (see also Figure 5 for the cycle 43) the result is, for the ascending passes and for the three antennae, an average increase of the signal around 0.07 dB. For the descending passes an average decrease of roughly 0.05 dB only for the aft antenna signal (the fore and mid signal show a more stable level). Therefore the change noted in the inter-beam calibration is mainly due to the aft antenna.

The following table summarize the biases computed in the antenna patterns:

Table 2: Antenna pattern biases (dB)

Antenna	Ascending passes 53-43	Ascending passes 52-42	Descending passes 53-43	Descending passes 52-42
Fore	+0.03	+0.08	0.0	-0.01
Mid	+0.05	+0.08	-0.01	-0.02
Aft	+0.05	+0.08	-0.05	-0.06

It is t is important to note that the shape of the antenna profiles (for all beams and passes) are very similar among the four cycles (42,43, 52 and 53) and this suggests that the change in the inter-beam calibration could be related with instrument evolution or platform event.

As reported in section 2.3.6 the monitoring of the evolution of the antennae temperature shows an increase of roughly 1.0 degree per year in the case of the fore and mid antenna while the aft anten-

na shows an increase of roughly 2.0 degrees per day. A possible correlation between the delta gamma nought (aft-fore) and the delta antenna temperature (at descending passes) has been investigated.

Figure 13 shows the result. As reported in the scatter-plot there is no correlation between the gamma nought bias and the temperature bias.

The evolution of the aft antenna signal during the descending passes could be related with instrument or mission events during that period. The most important are: the payloads switch-off to face out the Leonid meteorite shower (November 1999), a series of AMI emergency switch down anomalies and the AOCS mono-gyro configuration (February 2000). Unfortunately the noise present in the time series (see Figure 9) does not allow to estimate when the change occurred.

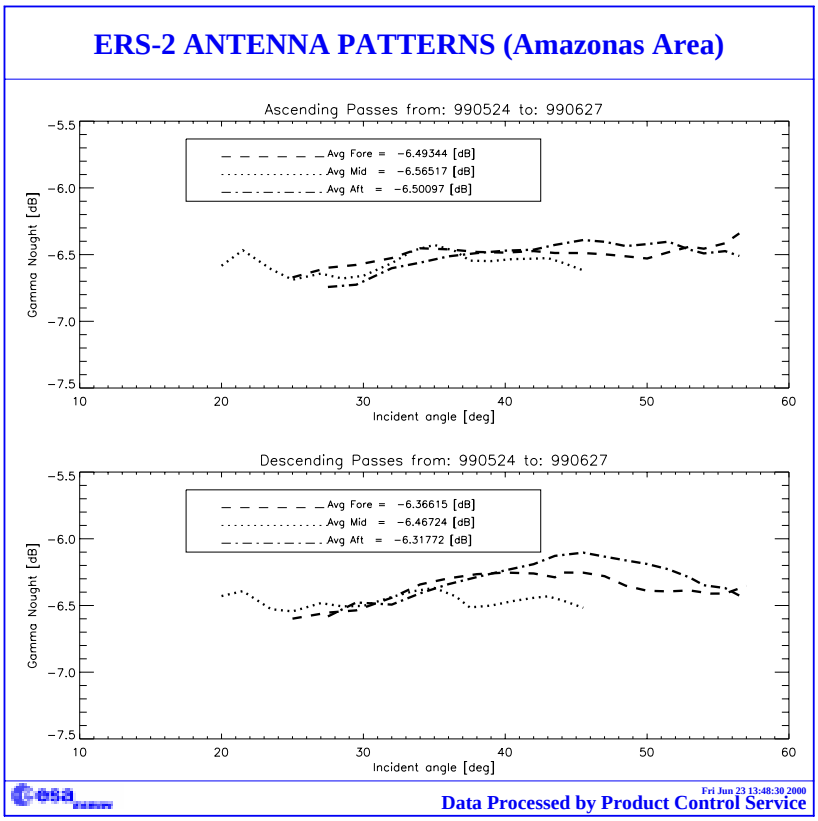

FIGURE 10. ERS-2 Scatterometer antenna patterns as function of the incidence angle: cycle 43

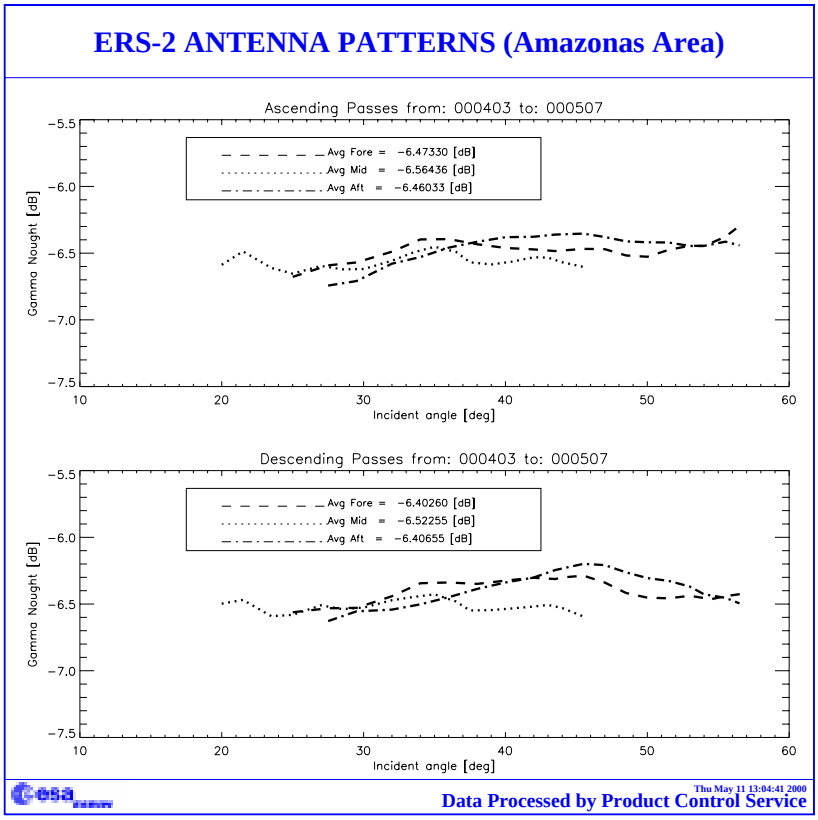

FIGURE 11. ERS-2 Scatterometer antenna patterns as function of the incidence angle: cycle 52.

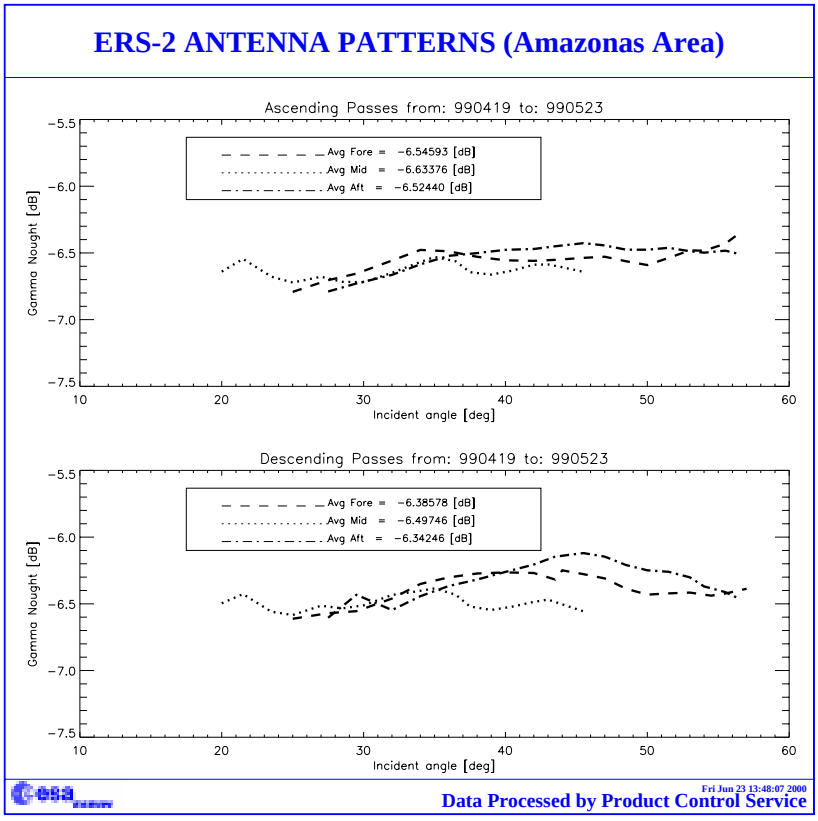

FIGURE 12. ERS-2 Scatterometer antenna patterns as function of the incidence angle: cycle 42.

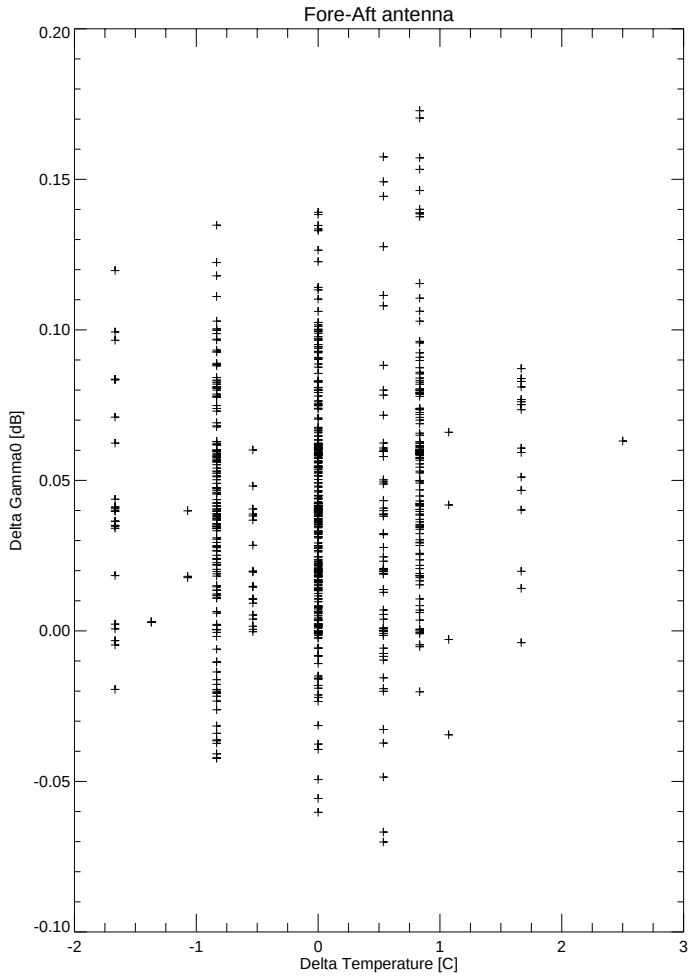

FIGURE 13. ERS-2 Scatterometer correlation between the gamma nought bias (aft-fore) and the antenna temperature bias (aft-fore) during the descending passes.

The mean and the standard deviation of gamma-nought are weekly computed directly using the Fast Delivery data. Figure 14 shows the evolution of the standard deviation since September 1996. The ascending passes show a gamma nought standard deviation more higher than the descending ones. This can be explained because at ascending passes the test site appears less homogeneous; in particular for some areas near the rivers (see Figure 20). The last plot in Figure 14 shows the number of valid measurements used to compute the statistics. It is clear the reduction of the number of valid observation since the beginning of 1999. This is due to an increase of SAR images acquired over the Amazon rain forest.

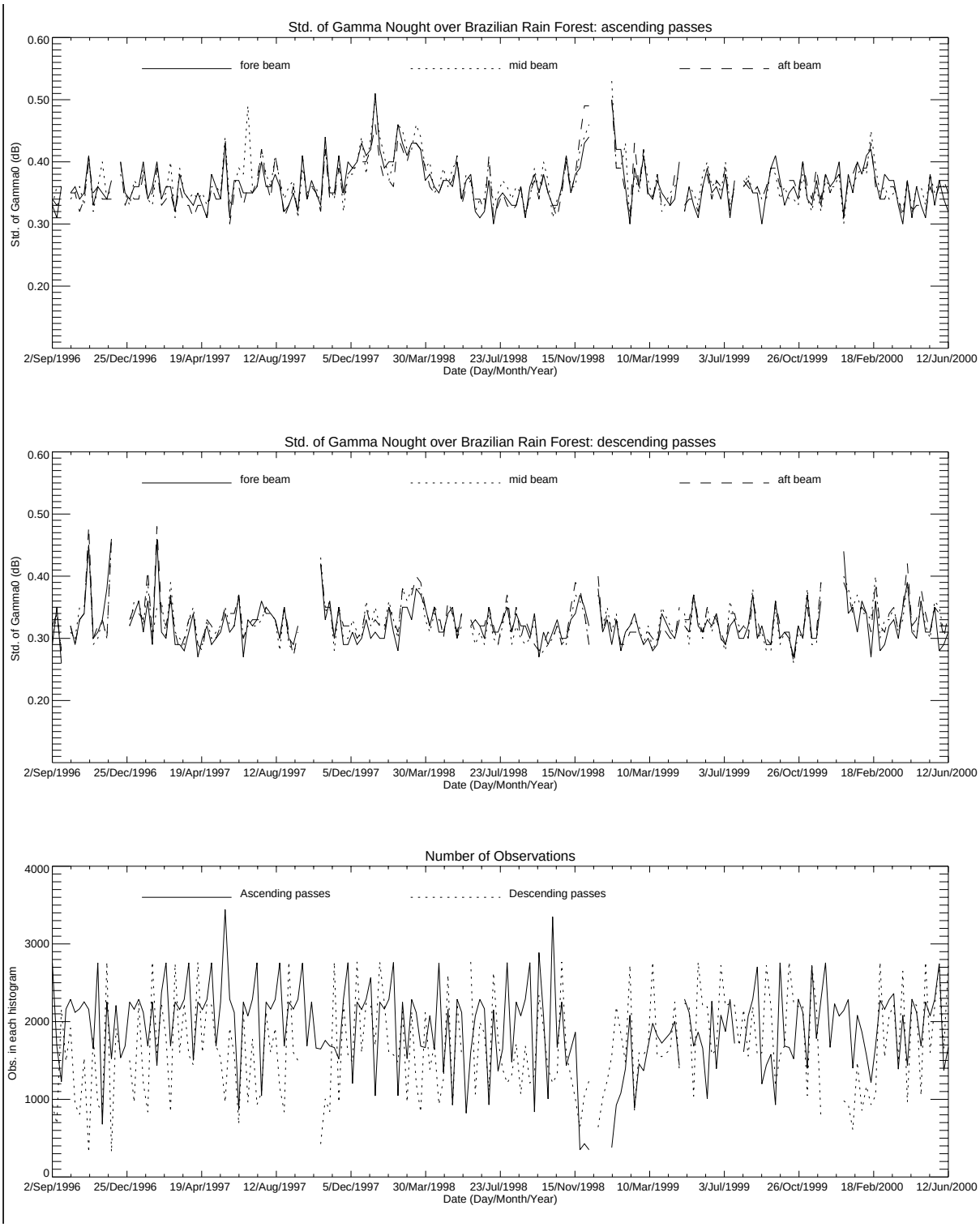

FIGURE 14. Gamma-nought histograms: weekly evolution of standard deviation. From up to down: ascending passes standard deviation, descending passes standard deviation, number of valid observations.

The Figures from 15 to 19 show the gamma-nought histogram over the Brazilian rain forest throughout cycle 53.

The histograms for the fifth week of the cycle (ascending passes) show slightly noise (geophysical). In the others cases, as expected, the histograms' shape shows a very sharp peak.

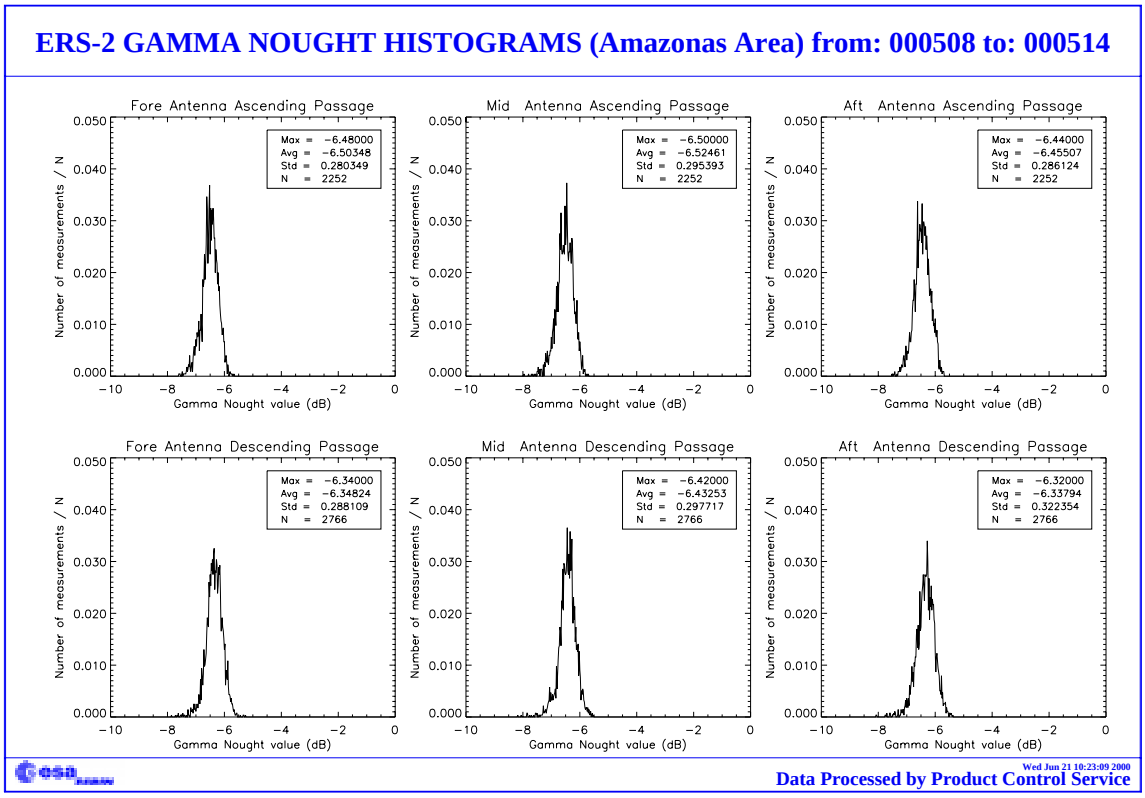

FIGURE 15. Gamma-nought histograms over Brazilian Rain forest: first week of the cycle 53.

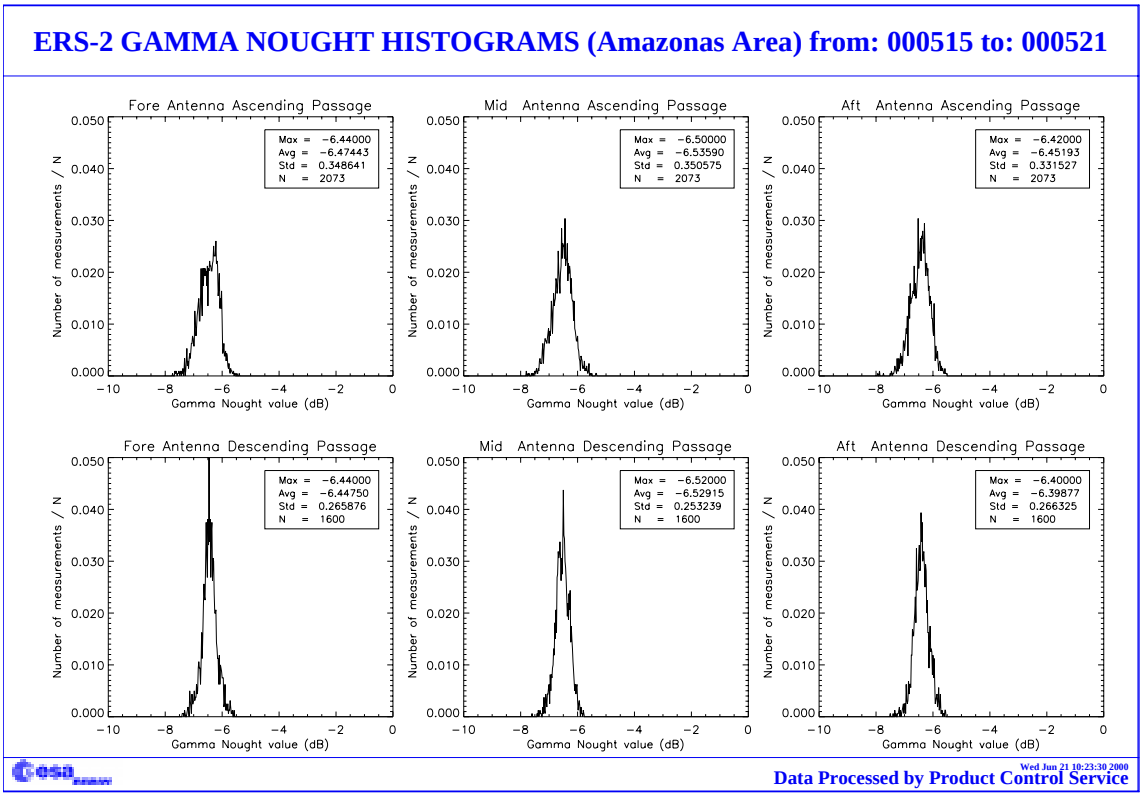

FIGURE 16. Gamma-nought histograms over Brazilian Rain forest: second week of the cycle 53.

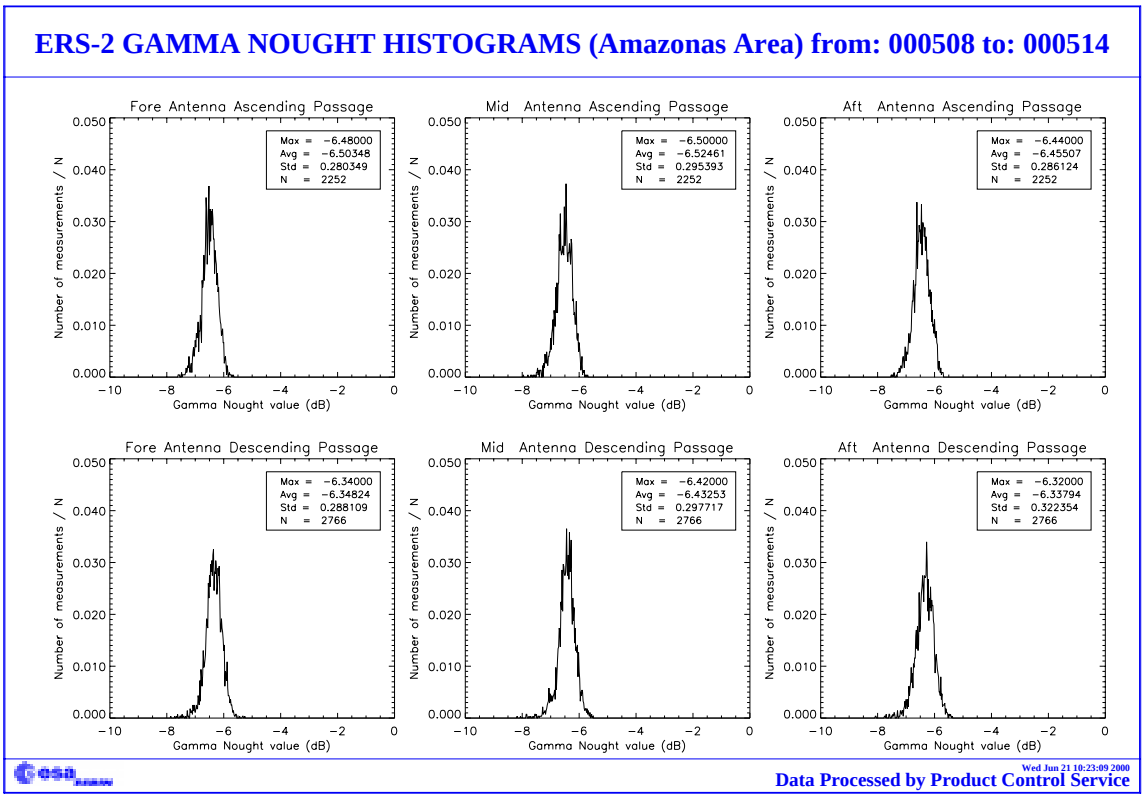

FIGURE 17. Gamma-nought histograms over Brazilian rain forest: third week of the cycle 53.

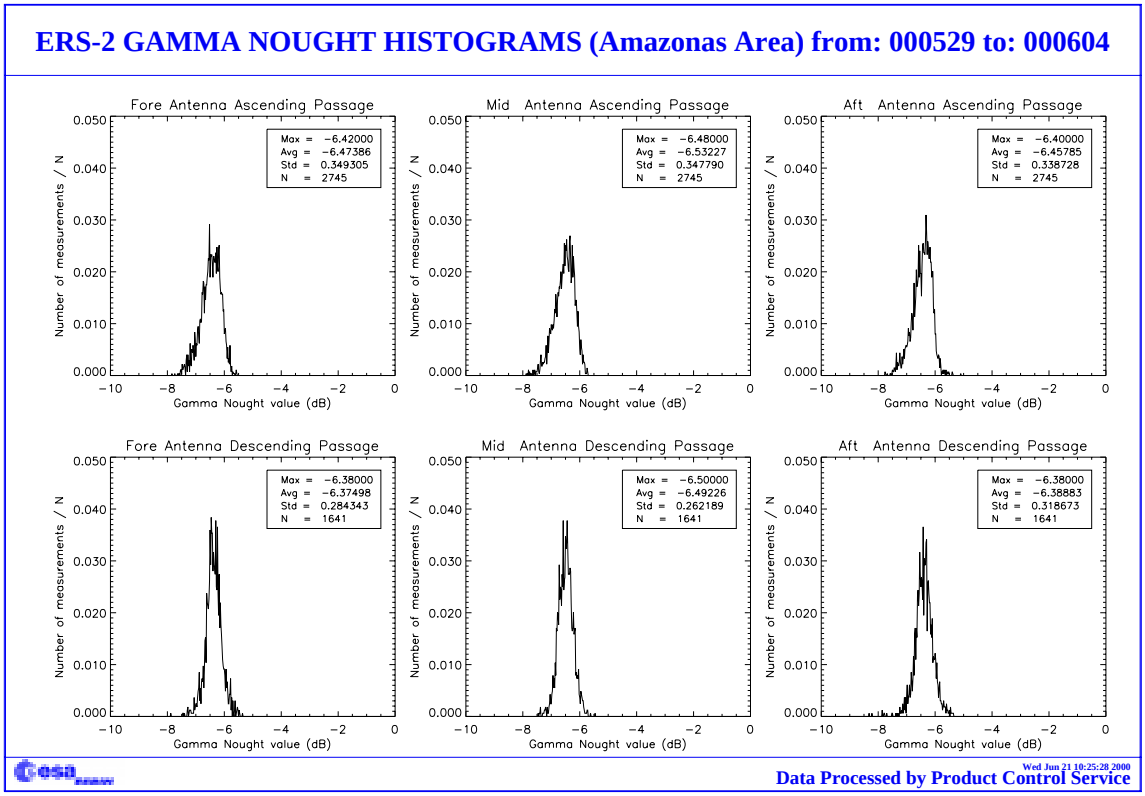

FIGURE 18. Gamma-nought histograms over Brazilian rain forest: fourth week of the cycle 53.

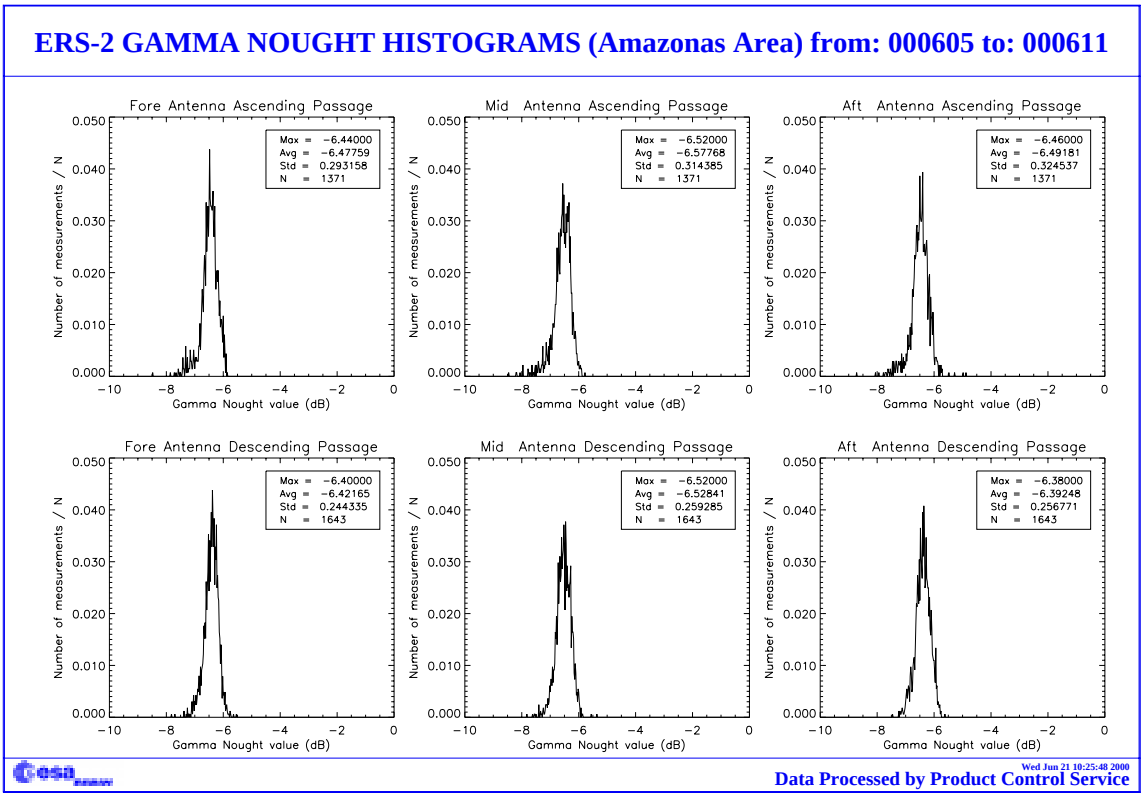

FIGURE 19. Gamma-nought histograms over Brazilian rain forest: fifth week of the cycle 53.

2.3.4 Gamma nought image of the reference area

The Figure 20 shows maps of the gamma nought over the Brazilian rain forest. This is the area where statistics are computed.

Each map has a resolution of 0.5 degrees in latitude and 0.5 degrees in longitude, roughly this is the instrument resolution at the latitude of the test site. In each resolution cell falls the average of all the valid observations available during one cycle (35 days).

From the figures no important changes happened in the test area during the cycle 53. As outlined in the previous reports the test area appears less homogenous at the ascending passes than in the descending ones. This seems due to the signal that comes from some areas near the rivers.These areas make the gamma nought histogram more noisy at ascending passes rather than at descending passes.

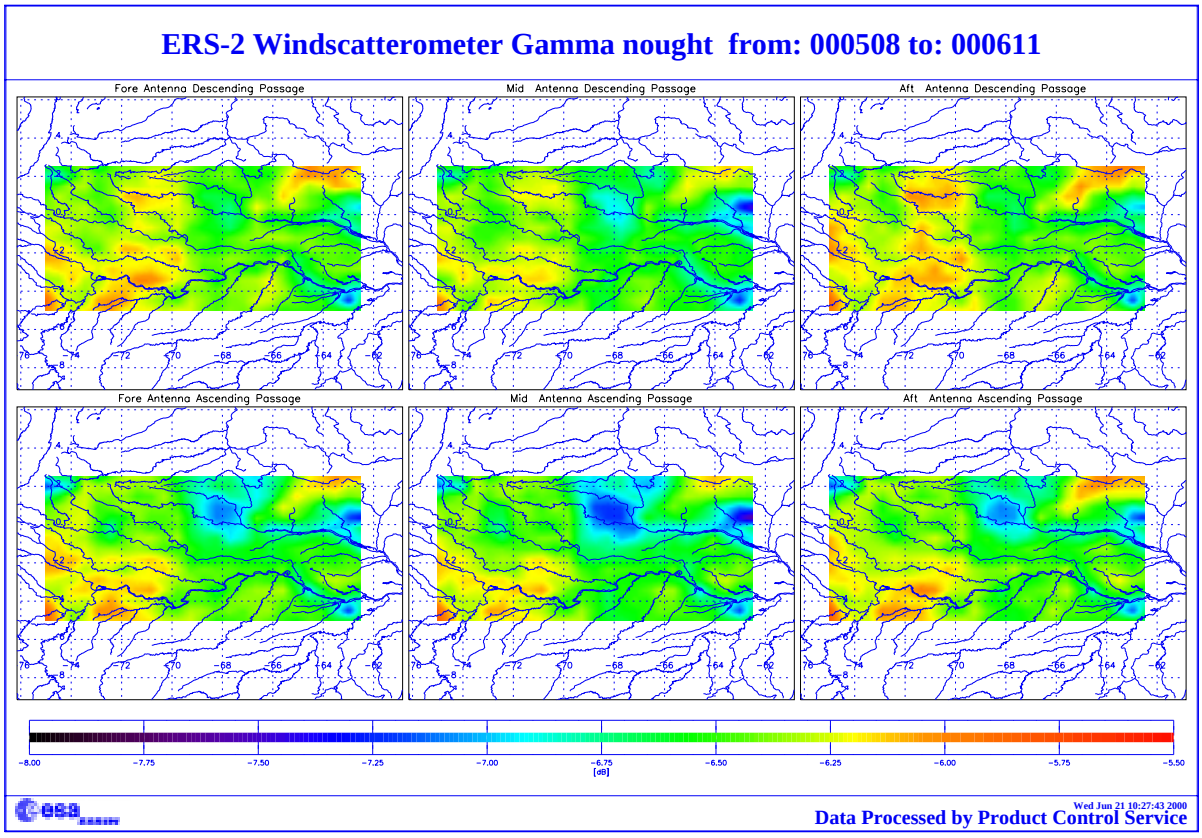

FIGURE 20. ERS-2 Scatterometer: gamma nought over the Brazilian rain forest cycle 53.

2.3.5 Sigma nought evolution

The Figures 21 and 22 show the evolution of the sigma nought (mid beam) over the reference area. The analysis is done per orbit and per node and the scope is to evaluate the stability of the sigma nought for each incidence angle. The relative track chosen are those where the number of valid measurements for each node (across track) is greater than 20.

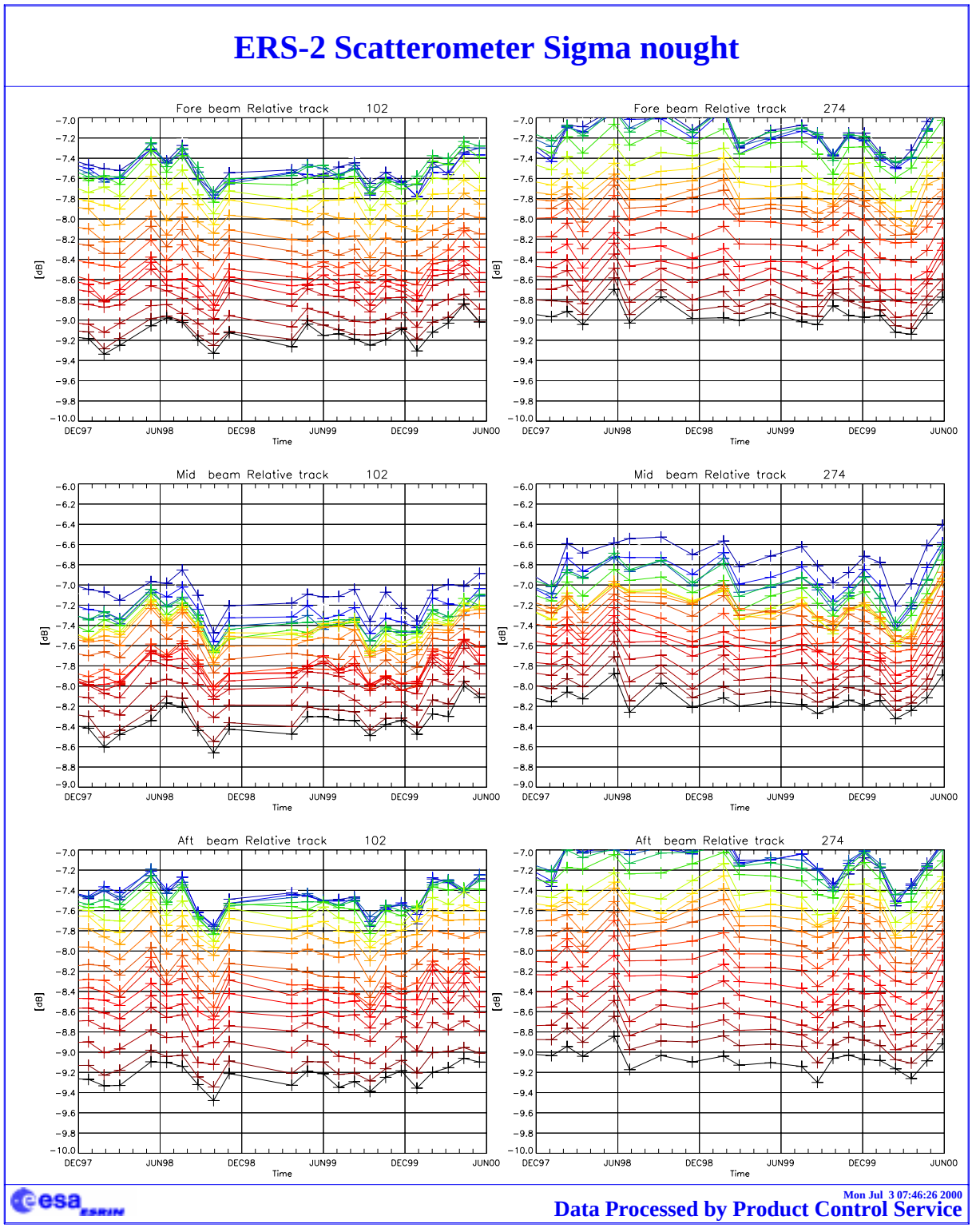

FIGURE 21. Sigma nought over the test area: ascending passes relative tracks 102 (left panels) and 274 (right panels); all nodes across the swath (since December 1997).

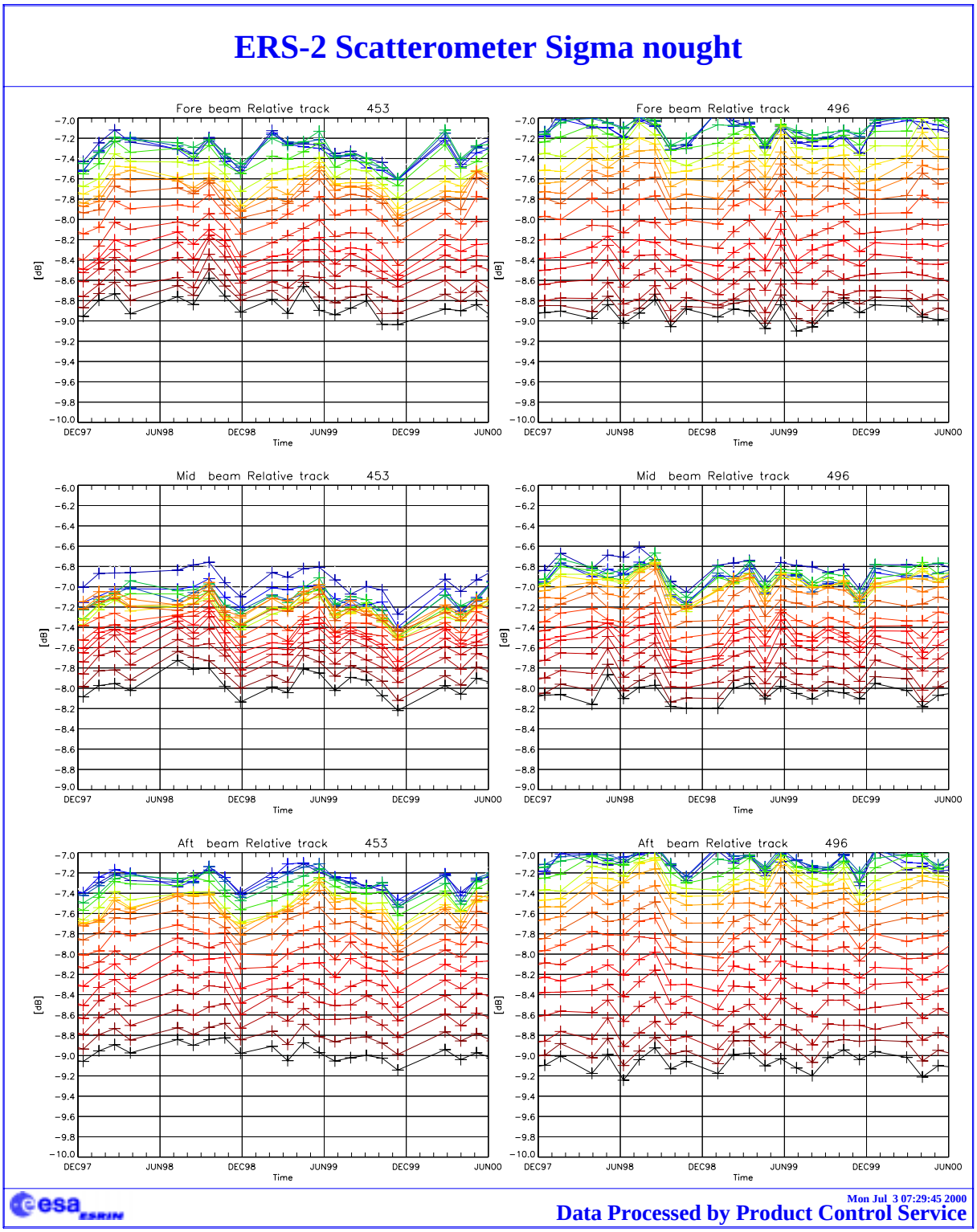

FIGURE 22. Sigma nought over the test area: descending passes relative tracks 453 (left panel) and 496 (right panel); all nodes across the swath (since December 1997).

The time series show a good correlation among the nodes (near and far range) and the stability of the sigma nought ranges from 0.2 to 0.5 dB depending on the node.

The result of the monitoring shows that the sigma nought is more stable during the descending passes. The relative track number 274 (ascending) shows an increase of the sigma nought (all nodes) during the last two cycles. The increase is roughly 0.4 dB and it is due to a geophysical effect.

2.3.6 Antenna temperature evolution over the Rain Forest

The monitoring of the antenna temperature over the Brazilian rain forest is performed by PCS. The antenna temperatures are retrieved from the satellite telemetry when the Scatterometer swath is over the test site and the instrument is active (AMI in wind only or wind/wave mode). The scope of this monitoring is to investigate a possible correlation between the antenna temperatures and the gamma-nought level. This correlation is not clear in the actual data because of the gamma nought variability of the selected area. A deep analysis is to be performed to better understand the facts.

The plots for the three beams and for the ascending, descending and all passes are in Figure 23. It is interesting to note that the annual variation is due to the earth inclination and that the antenna temperatures have an increase of roughly 1.0 degree per year in the case of the mid and fore antenna; 2 degrees per year for the aft antenna.

This temperature increase could be related to the degradation of the antennae protection film.

The result of the monitoring during the cycle 53 shows that the antenna temperature evolution is within the nominal range.

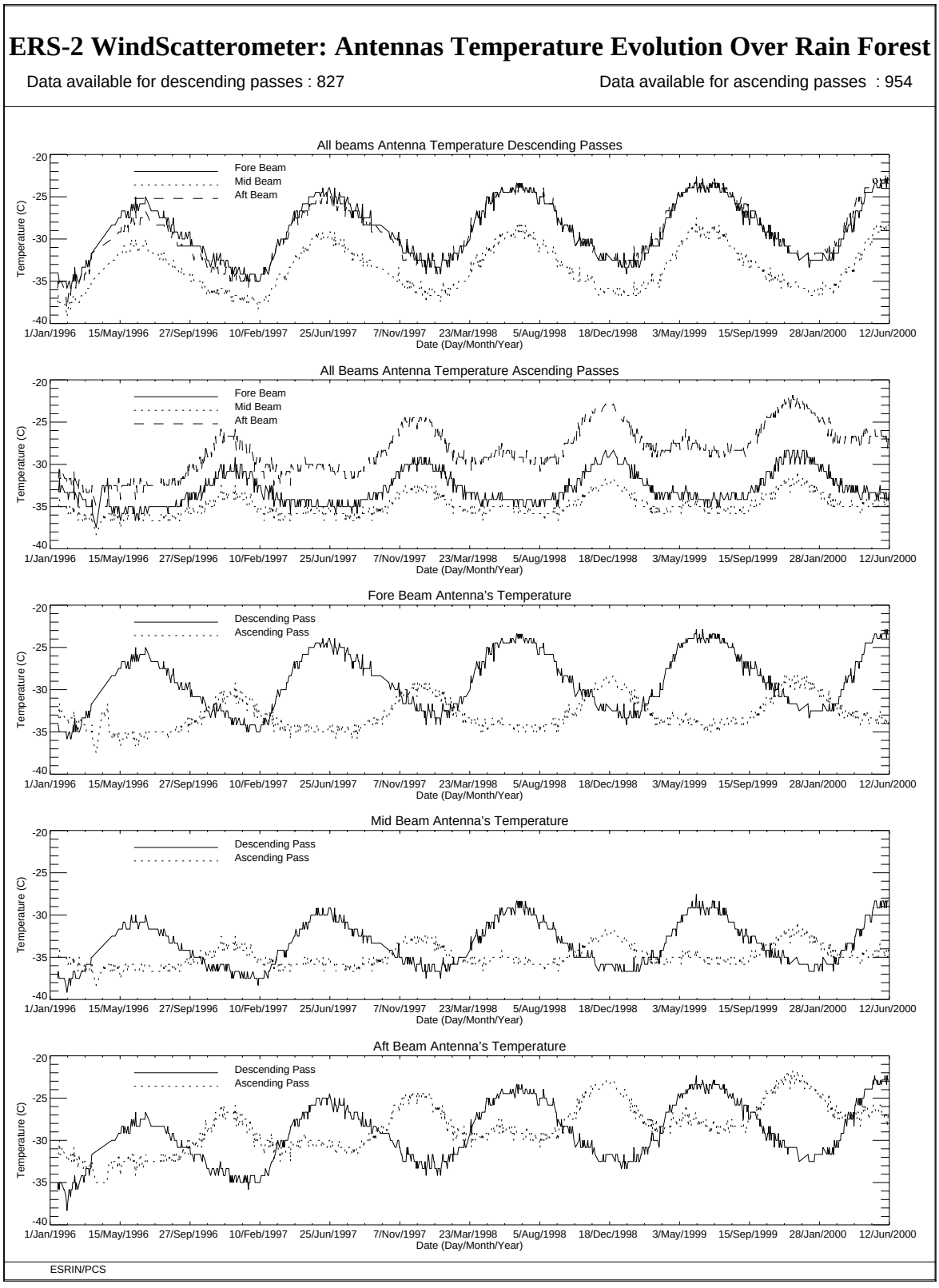

FIGURE 23. ERS-2 Scatterometer: evolution of the antenna temperatures over the Brazilian rain forest.

3.0 Instrument performance

The instrument status is checked by monitoring the following parameters:

- Centre of Gravity (CoG) and standard deviation of the received signal spectrum. This parameter is useful for the monitoring of the orbit stability, the performances of the doppler compensation filter, the behaviour of the yaw steering mode and the performances of the devices in charge for the satellite attitude (e.g. gyroscopes, earth sensor).
- Noise power I and Q channel.
- Internal calibration pulse power.

the latter is an important parameter to monitor the transmitter and receiver chain, the evolution of pulse generator, the High Power Amplifier (HPA), the Travelling Wave Tube (TWT) and the receiver.

These parameters are extracted daily from the UWI products and averaged. The evolution of each parameter is characterised by a least square line fit. The coefficients of the line fit are printed in each plot.

3.1 Centre of gravity and standard deviation of received power spectrum

The Figure 24 shows the evolution of the two parameters for each beam.

The tendency from the beginning of the mission to the operation with the new Attitude On-board Control System (AOCS) configuration (7th February 2000) is a clear and regular increase of the Centre of gravity (CoG) of received spectrum for the three antennae. An increase of roughly 200 Hz was observed at the end of the AOCS qualification period. After the AOCS commissioning phase this parameter further evolved. In particular this bias was reduced by 100 Hz on 22nd March and was close to zero on the end of cycle 51 (3rd April 2000). During the cycle 52 the CoG of the received spectrum had a regular increase while for cycle 53 the result was more stable (see also Figure 25).

The old AOCS configuration (one Digital Earth Sensor - DES, one Digital Sun Sensor - DSS and 3 gyros) is no more considered safe because 3 of the six gyros on-board are out of order or very noisy. The new attitude control configuration is designed to pilot the ERS-2 using only one gyro plus the DES and the DSS modules. Scope of this new configuration is to extend the satellite lifetime by using the available gyros one at the time.

The evolution of the standard deviation of the CoG of the received spectrum is more stable apart from the change occurred on 26th, October 1998. On October 26th, 1998 the standard deviation of the CoG had, on average, a decrease of roughly 100 Hz for the fore and aft antenna and of roughly 30Hz for the mid antenna. This change is linked with the increase of the transmitted power (see Section 3.3).

Others changes in the AOCS configuration are recognised in Figure 24. The two steps observed at the beginning of the plots of the CoG (see Figure 24) are due to a change in the pointing subsystem (DES reconfiguration) side B instead of side A after a depointing anomaly (see table 3 for the

list of the AOCS depointing anomaly occurred during the ERS-2 mission). The first change is from 24th, January 1996 to 14th, March 1996, the second one is from 14th February 1997 to 22nd April 1997. During these periods side B was switched on. It is important to note that during the first time a clear difference in the CoG of the received spectrum is present only for the Fore antenna (an increase of roughly 100 Hz) while during the second time the change has affected all the three antennae (roughly an increase of 200 Hz, 50 Hz and 50 Hz for the fore, mid and aft antenna respectively).

Table 3: ERS-2 Scatterometer AOCS depointing anomaly

From	To
24th January 1996 9:10 a.m.	26th January 1996 6:53 p.m
14th February 1996 1:25 a.m.	15th February 1996 3:44 p.m
3rd June 1998 2:43 p.m.	6th June 1998 12:47 a.m.
1st September 1999 8:50 a.m.	2nd September 1999 1:28 a.m.

The Figure 24 shows also when the satellite was operated in Fine Pointing Mode (FPM) or the on-board doppler compensation was missing. These events are related with the large peaks in the CoG of the received spectrum plots (fore and aft antenna) and are listed in Table 4.

Table 4: ERS-2 Scatterometer anomalies in the CoG fore and aft antenna

Date	Reason
26th and 27th September 1996	missing on-board doppler coefficient (after cal. DC converter test period)
6th and 7th June 1998	no Yaw Steering Mode (after depointing anomaly)
2nd and 3rd December 1998	missing on-board doppler coefficients (after AMI anomaly 228)
16th and 17th February 2000	Fine Pointing Mode (FPM) (due to AOCS mono-gyro qualification period)
14th April 2000	Fine Pointing Mode (FPM)
30th May 2000	Fine Pointing Mode (FPM)

The peaks shown in the plot of mid beam standard deviation of the CoG of the received spectrum are linked to the satellite manoeuvres and AOCS depointing anomaly.

An analysis of the evolution of the doppler frequency as function of the ascending node time has been carried out. The scope of the analysis was to better understand the evolution of the CoG of the received spectrum after the mono-gyro qualification period.

Figures 26 shows the result for the cycle 53. In the figures are plotted, with different colours, the three days averaged CoG of the received spectrum (mid antenna) as time function from the ascending node (time = 0). Each unit of the X axis is 5 seconds from the ascending node while the Y axis is the frequency in Hz. The curves are obtained filtering the evolution of the CoG of the received spectrum throughout the orbit.

The large variation of the doppler frequency on 30th May 2000 is because the satellite was in FPM.

The cycle 53 shows a very stable result. The maximum of the doppler frequency around the end of orbit (roughly after 5200 s. from the ascending node) was more stable with reference to the previous cycle. The agreement of the Doppler frequency with the reference sinusoidal pattern is good. The main difference between the evolution of the doppler frequency and the reference sinusoidal pattern is around 4500 s. after the ascending node.

ERS-2 WindScatterometer: DOPPLER COMPENSATION Evolution (UWI)

Least-square poly. fit fore beam	Center of gravity = -313.5 +(0.1167)*day	Standard Deviation = 4242.2 +(0.0559)*day
Least-square poly. fit mid beam	Center of gravity = -647.8 +(0.1087)*day	Standard Deviation = 5127.5 +(0.0105)*day
Least-square poly. fit aft beam	Center of gravity = -364.7 +(0.0954)*day	Standard Deviation = 4368.1 +(0.0400)*day

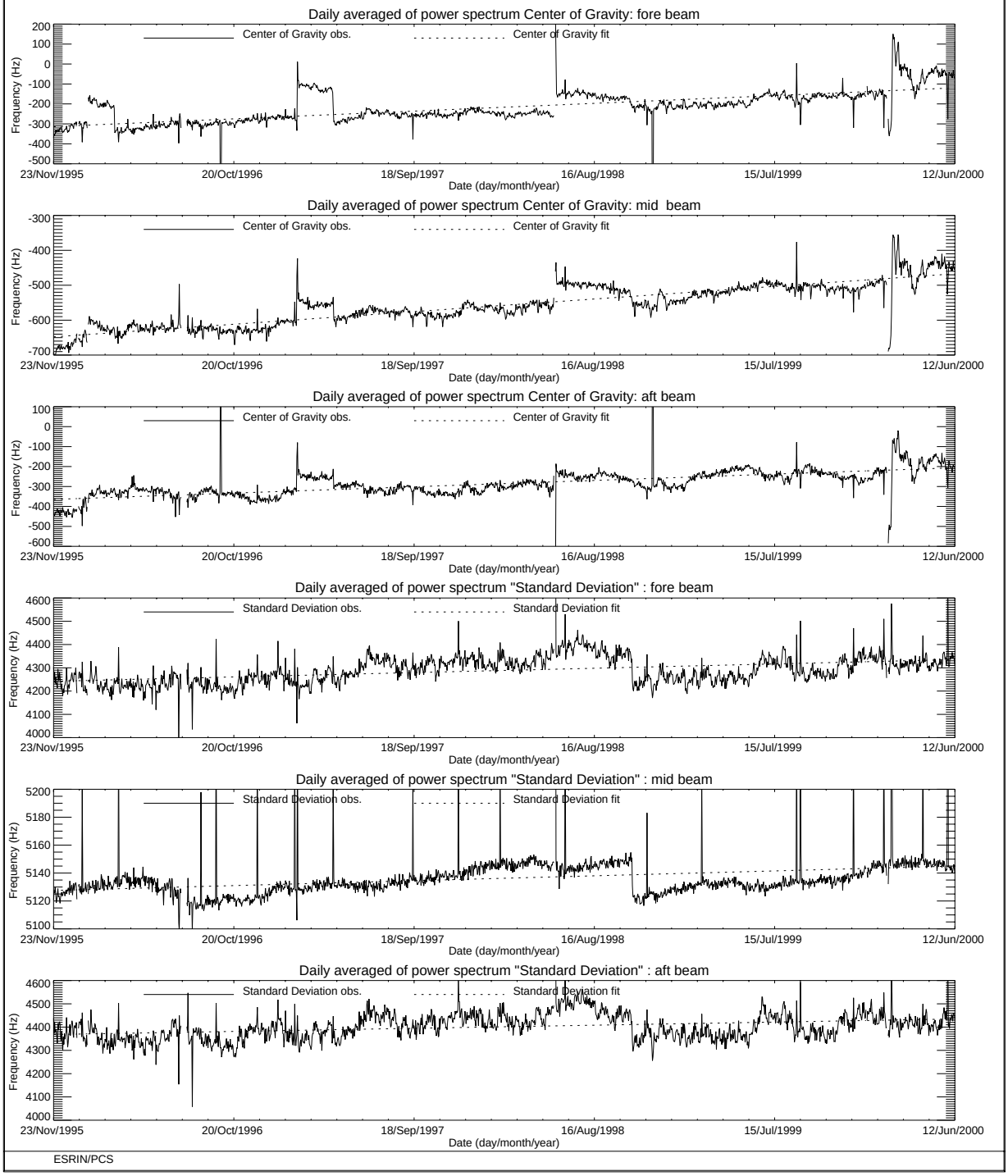

FIGURE 24. ERS-2 Scatterometer: Centre of Gravity and standard deviation of received power spectrum since the beginning of the mission.

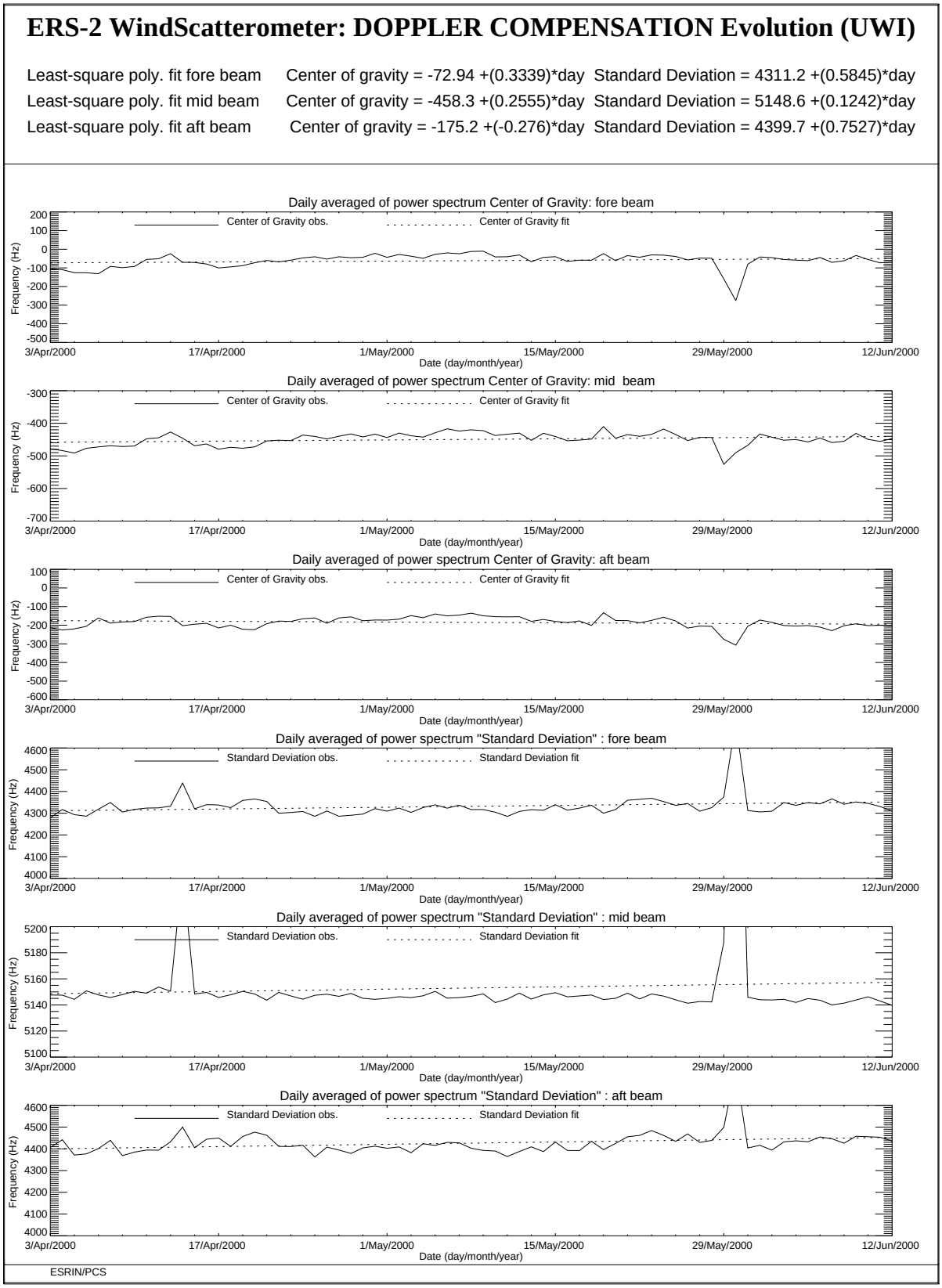

FIGURE 25. ERS-2 Scatterometer: Centre of Gravity and standard deviation of received power spectrum during the cycle 52 and cycle 53.

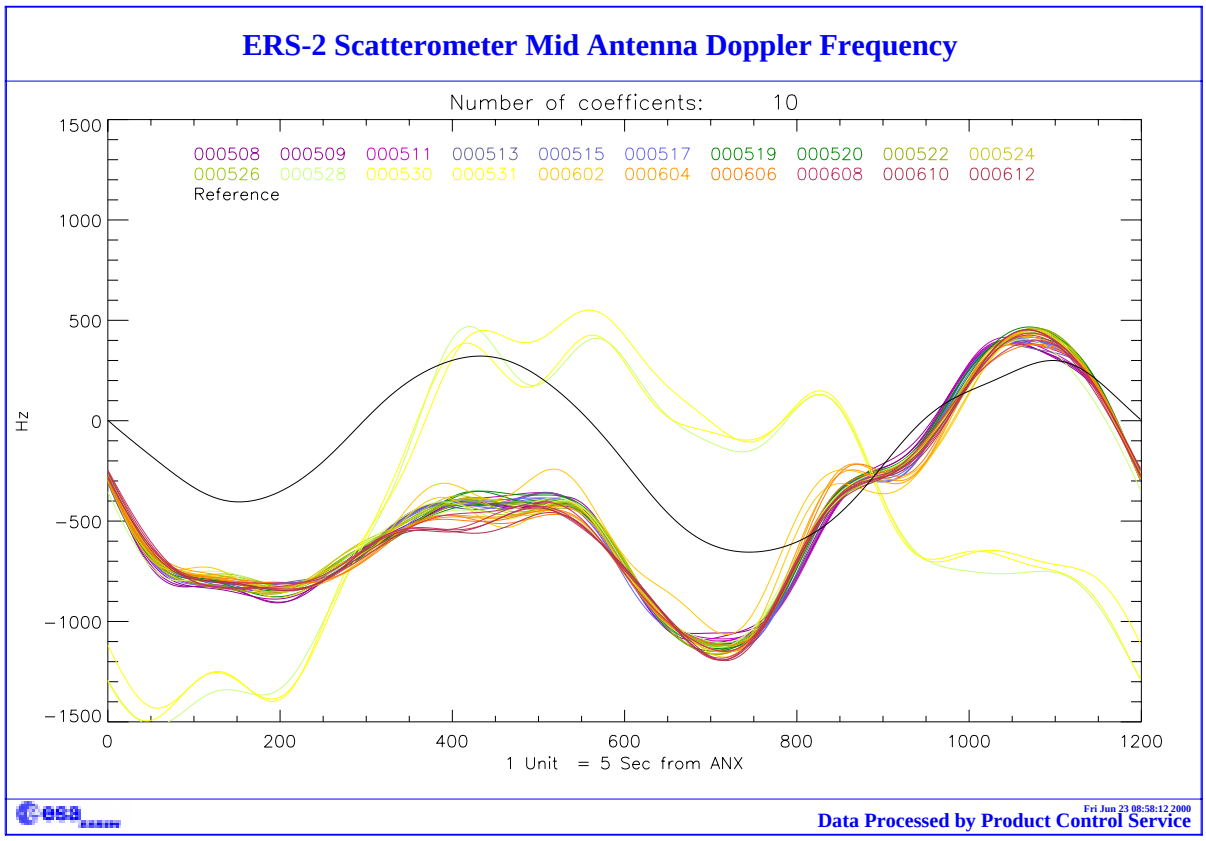

FIGURE 26. Low pass filtered evolution of the Mid beam CoG as function of ascending node time (1 unit 5 s.). Cycle 53

3.2 Noise power level I and Q channel

The results of the monitoring are shown in Figure 27. The first set of three plots presents the noise power evolution for the I channel while the second set shows the Q channel. The noise level is less than 1 ADC Unit for the fore and aft signals and is negligible for the mid one. From the plots one can see that the noise level is more stable in the I channel than in the Q one. The PCS suspects that an explanation should be found in the different position of the receivers, in particular it seems that the Q one is closer to the ATSR-GOME electronics. A confirmation of this hypothesis has been asked to ESTEC.

Since 5th December 1997 some high peaks appear in the plots. These high values for the daily mean are due to the presence for these special days of a single UWI product with an unrealistic value in the noise power field of its Specific Product Header. The analysis of the raw data used to generate these products lead in all cases to the presence of one source packet with a corrupted value in the noise field stored into the source packet Secondary Header. Table 5 presents the list of the UWI products affected by a corrupted noise field and disseminated during cycle 53.

Table 5: UWI products with noise field corrupted (cycle 53)

Noise Field corrupted	Noise value (ADC Unit)	Acquisition Time
None	-	-

The reason why noise field corruption is beginning from 5th December 1997 is at present unknown. It is interesting to note that at the beginning of December 1997, we started to get as well the corruption of the Satellite Binary Times (SBTs) stored in the EWIC product. The impact in the fast delivery products was the production of blank products starting from the corrupted EWIC until the end of the scheduled stop time. A change in the ground station processing in March 1998 overcame this problem.

Since 9th August 1998 some periods with a clear instability in the noise power have been recognised. Table 6 gives the detailed list.

Table 6: ERS-2 Scatterometer instability in the noise power

From	To
9th August 1998	26th October 1998
29th November 1998	6th December 1998
23rd December 1998	24th December 1998
7th June 1999	10th June 1999
17th August 1999	22nd August 1999
8th September 1999	9th September 1999
3rd October 1999	8th October 1999
16th October 1999	18th October 1999
26th October 1999	28th October 1999

From	To
25th December 1999	2nd January 2000
10th February 2000	11th February 2000
19th March 2000	26th March 2000

To better understand the instability of the noise power the PCS has carried out investigations in the scatterometer raw data (EWIC) to compute the noise power with more resolution. The result is that for the orbits affected by the instability the noise power had a decrease of roughly 0.7 dB for the fore and aft signals and a decrease of roughly 0.6 dB in the mid beam case (see the report for the cycle 42).

The decrease of the noise power during the orbits affected by the instability is comparable with the decrease of the internal calibration level that occurred during the same orbits. The reason of this instability (linked to the AMI anomalies) is still under investigation. A plot that shows the correlation among the noise power, the internal calibration level and the AMI anomaly is reported in section 3.3.

Figure 28 shows the evolution of the noise power since 26th October when 2 dB were added to the transmitted power. The periods with the instability in the noise power are clear shown in the plots in particular for the fore and aft beam signals.

During cycle 53 the evolution of the noise power evolution was stable.

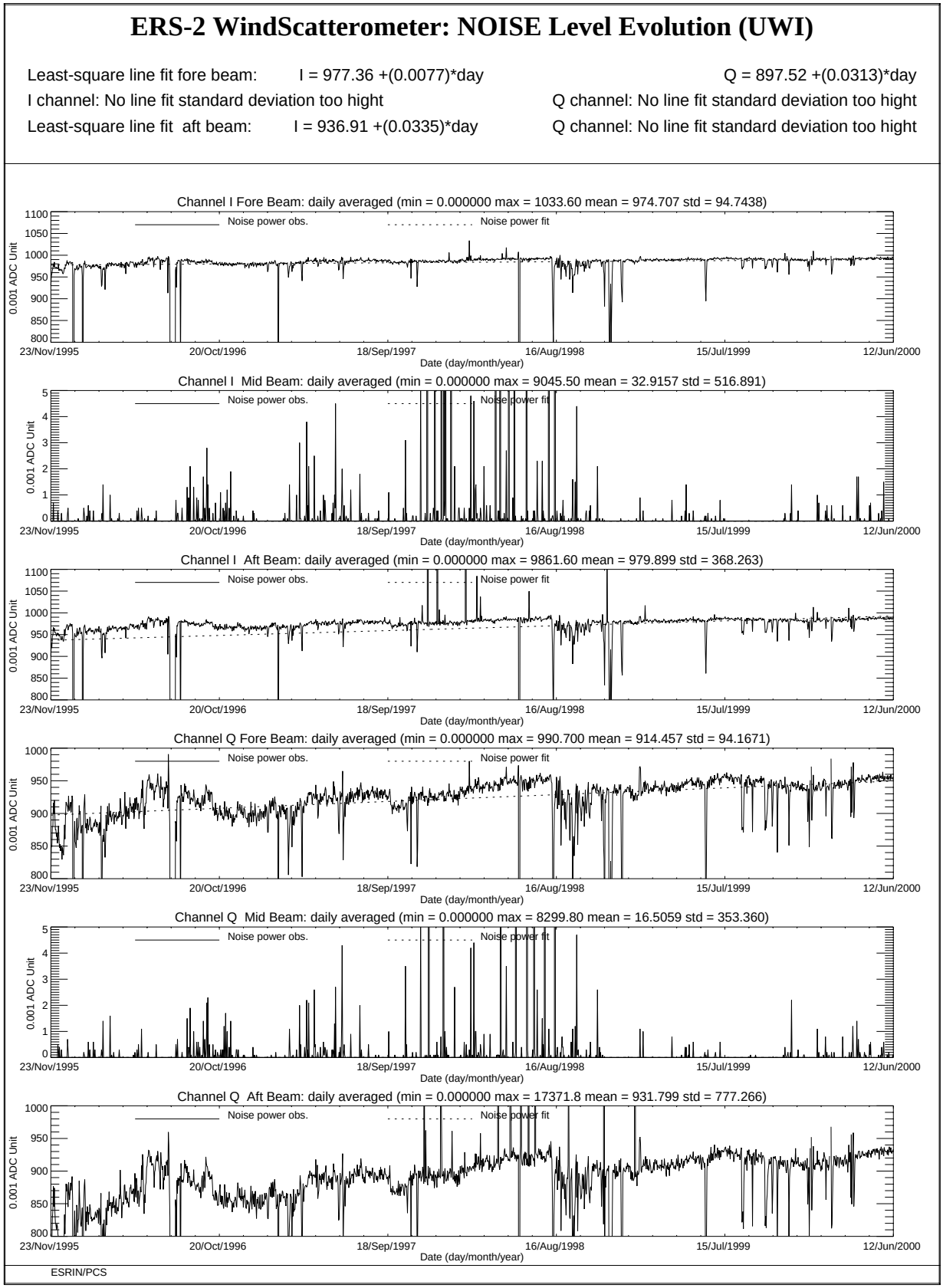

FIGURE 27. ERS-2 Scatterometer: noise power I and Q channel since the beginning of the mission.

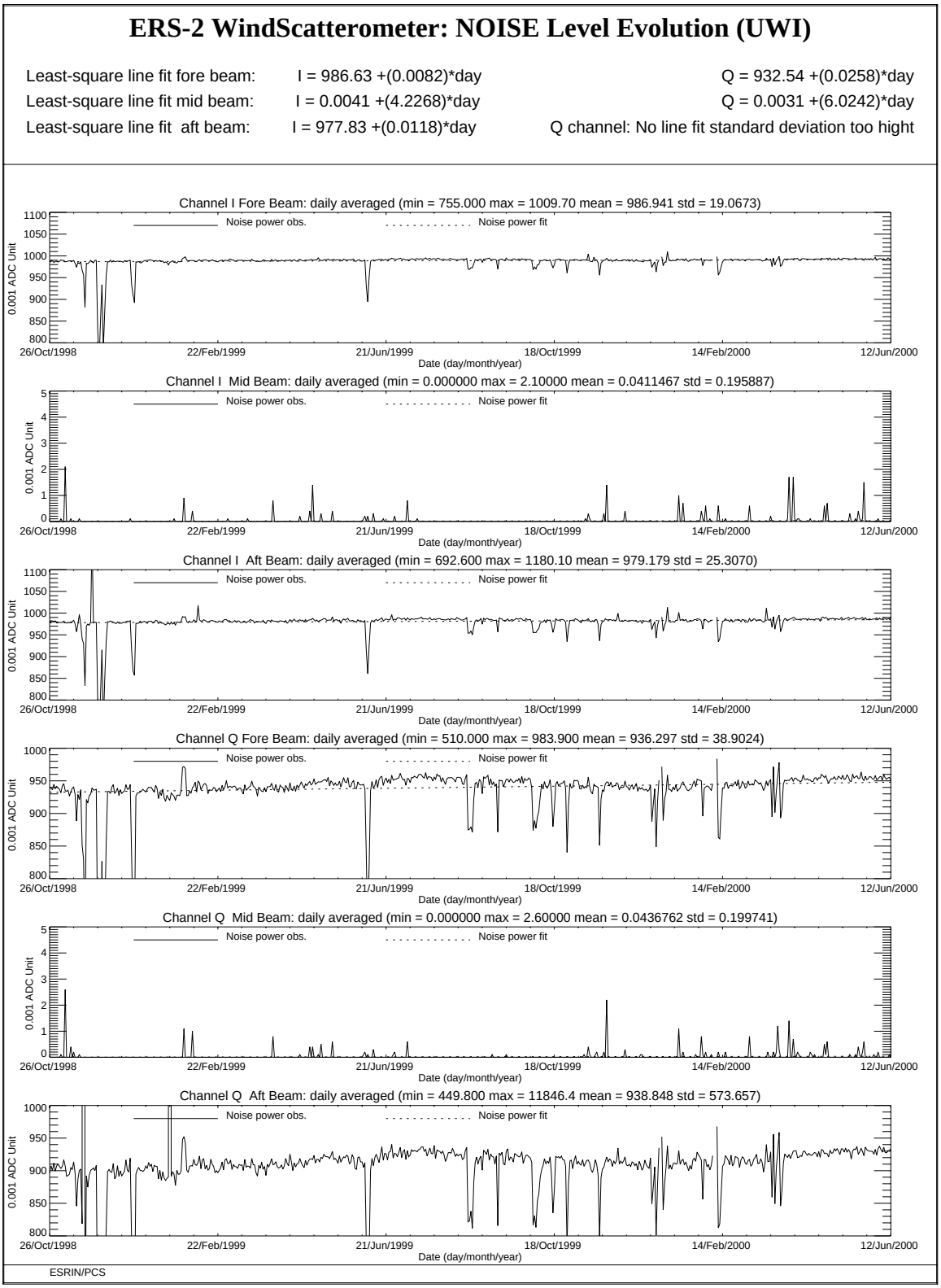

FIGURE 28. ERS-2 Scatterometer: noise power I and Q channel since 26th October 1998 when the transmitted power was increased by 2 dB.

3.3 Power level of internal calibration pulse

For the internal calibration level, the results, since the beginning of the mission, are shown in Figure 30.

The high value of the variance in the fore beam until August, 12th 1996 is due to the ground processing. In fact all the blank source packets ingested by the processor were recognized as fore beam source packets with a default value for the internal calibration level. The default value was applicable for ERS-1 and therefore was not appropriate for ERS-2 data processing. On August 12th, 1996 a change in the ground processing LUT overcame the problem.

Since the beginning of the mission a power decrease is detected. The power decrease is regular and affects the AMI when it is working in wind-only mode, wind/wave mode and image mode indifferently.

The reason is that the TWT is not working in saturation, so that a variation in the input signal is visible in the output. The variability of the input signal can be two-fold: the evolution of the pulse generator or the tendency of the switches between the pulse generator and the TWT to reset themselves into a nominal position. These switches were set into an intermediate position in order to put into operation the scatterometer instrument (on 16th November 1995).

After the change of the calibration subsystem on August 6th, 1996 the decrease is more evident and it is estimated in 0.09 dB per cycle (0.0025 dB/day).

On 26th October 1998 (cycle 37) to compensate for this decrease, 2.0 dB were added to the Scatterometer transmitted power and this explains the large step shows in Figure 29 and Figure 30. After that day the power decrease is on average 0.08 dB per cycle (0.0022 dB/day).

It is important to point out the efficiency of the internal calibration for keeping the absolute calibration level stable. In fact, no important change is noted in the monitoring of the gamma-nought level over the Brazilian rain forest during the power decrease and after the increase of the transmitted power (see section 2.0).

Since 9th August 1998 the internal calibration level shows an instability. This instability is very well correlated with the fluctuations observed in the noise power as outlined in section 3.2.

Figure 29 shows the daily average of the internal calibration and the noise power from 1st August 1998 to 12th June 2000. In the figure are also reported the anomalies that affected the AMI (the triangles in the plot) and the days when the instability was very strong (asterisks in the plot).

From Figure 29 it seems that there is a clear correlation between the instability (noise and calibration level) and the AMI anomalies.

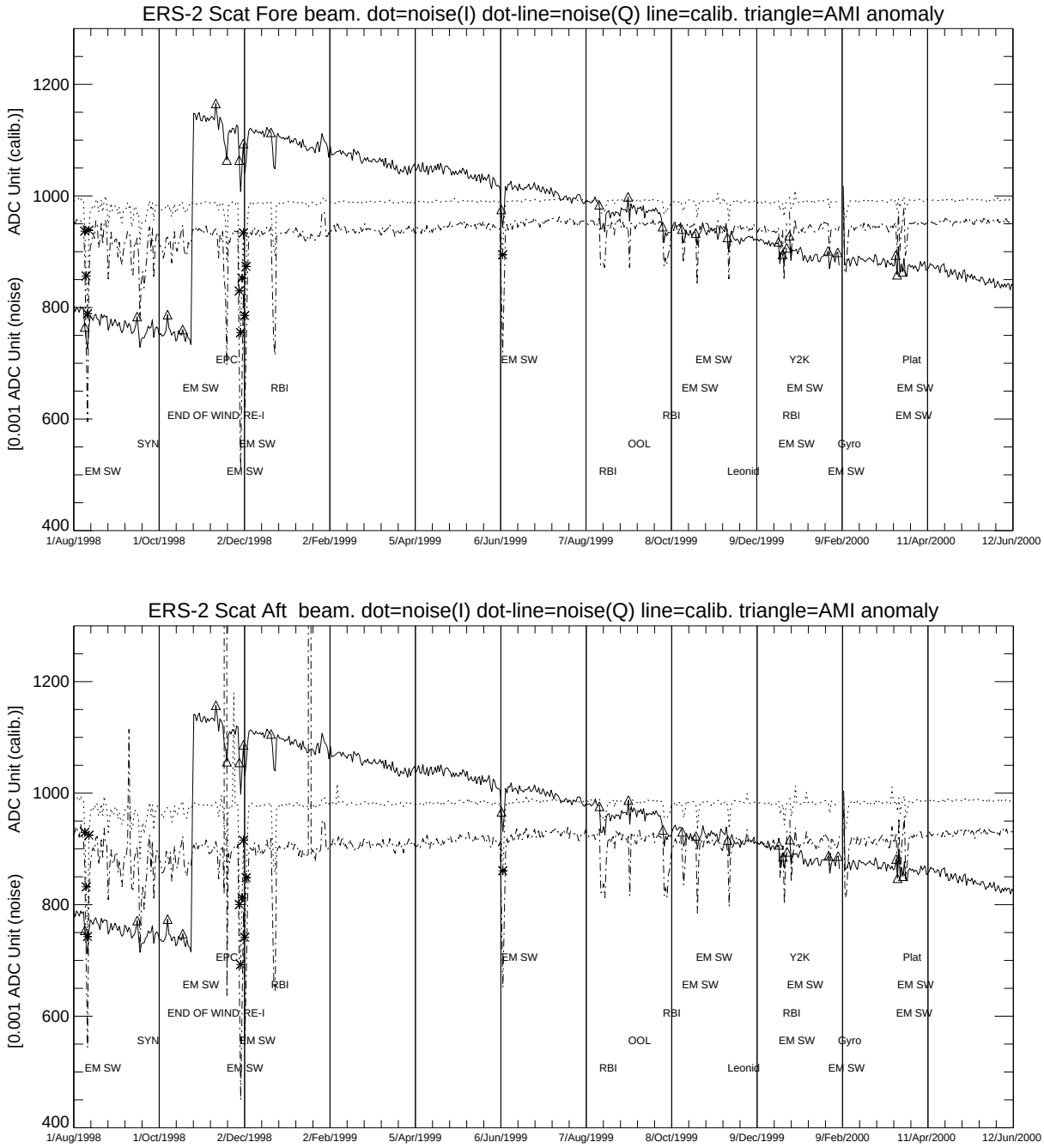

FIGURE 29. ERS-2 Scatterometer: noise power (I and Q channel) and internal calibration power evolution from 1st August 1998 to 8th May 2000. Upper panel fore antenna, lower panel aft antenna.

During the cycle 53 the internal calibration level had, on average, a power decrease of 0.1 dB. This value is very close to the one computed for the previous cycle.

Apart from the AMI anomalies the power decrease since 26th October 1998 is regular and it is on average 0.08 dB per cycle as shown in Figure 31.

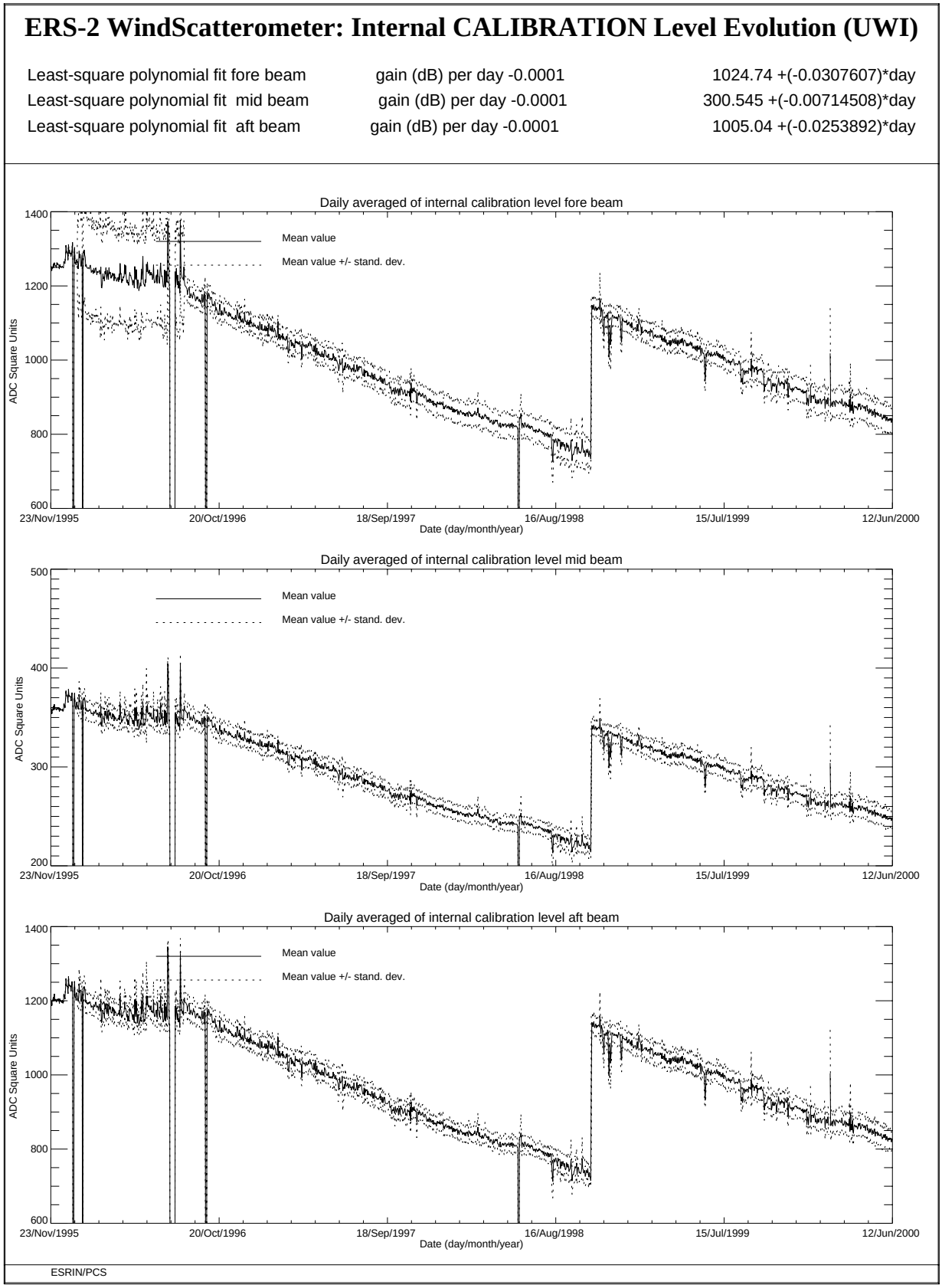

FIGURE 30. ERS-2 Scatterometer: power of internal calibration pulse since the beginning of the mission.

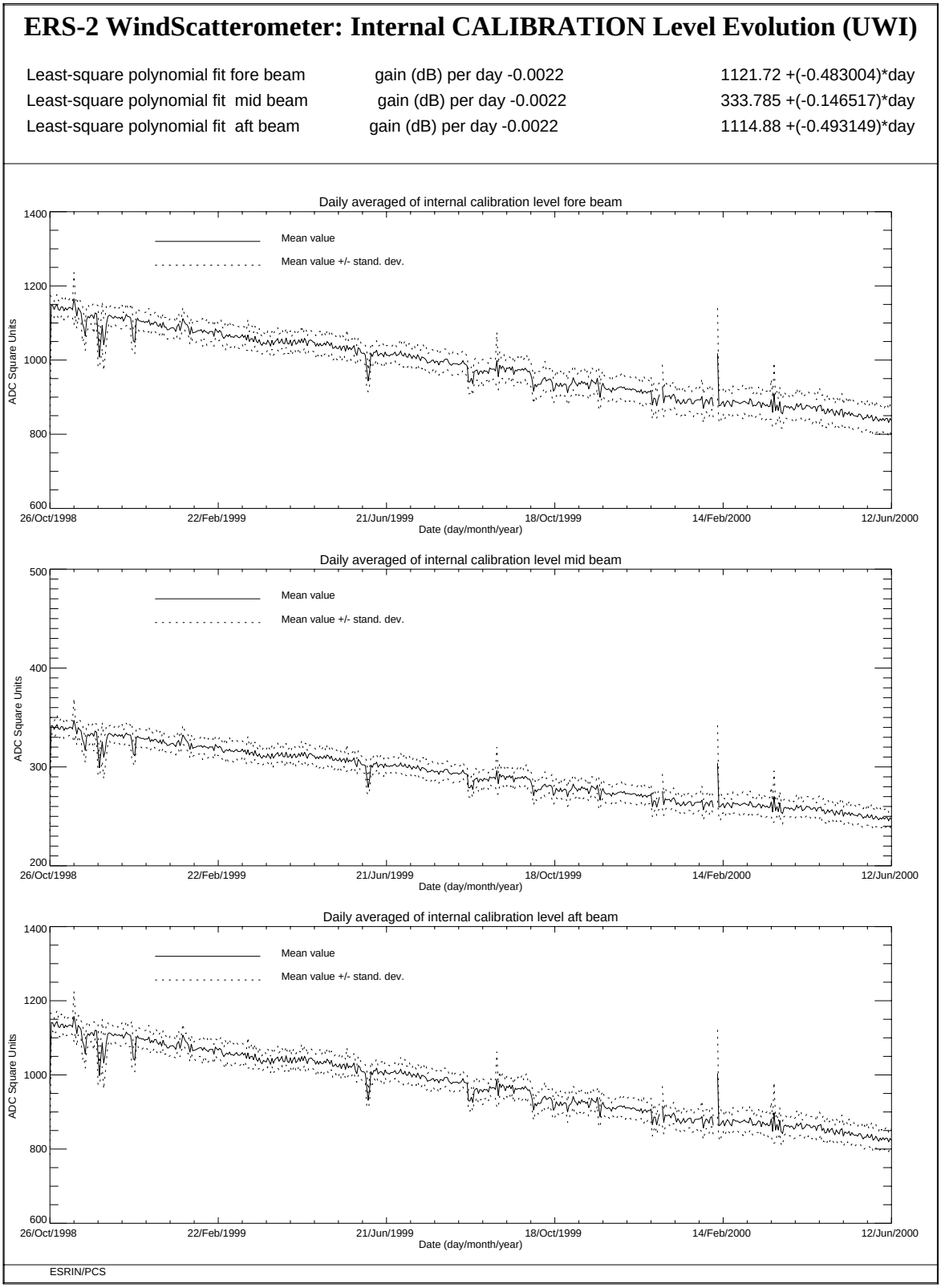

FIGURE 31. ERS-2 Scatterometer: power of internal calibration level since 26th October 1998 when the transmitted power was increased by 2.0 dB.

4.0 Products performance

One of the most important point in the monitoring of the products performance is their availability. The Scatterometer is a part of ERS payload and it is combined with a Synthetic Aperture Radar (SAR) into a single Active Microwave Instrument (AMI). The SAR users requirements and the constraints imposed by the on-board hardware (e.g. amount of data that can be recorded in the on-board tape) set rules in the mission operation plan.

The principal rules that affected the Scatterometer instruments are:

- over the Ocean the AMI is in wind/wave mode (scatterometer with small SAR imagettes acquired every 30 sec.) and the ATSR-2 is in low rate data mode.
- over the Land the AMI is in wind only mode (only scatterometer) and the ATSR-2 is in high rate mode. (Due to on board recorder capacity, ATSR-2 in high rate is not compatible with Sar wave imagette acquisitions.)

This strategy preserves the Ocean mission.

Moreover:

- the SAR images are planned as consequence of users' request.

These rules have an impact on the Scatterometer data availability as shown in Figure 32.

Each segment of the orbit has different colour depending on the instrument mode: brown for wind only mode, blue for wind-wave mode and green for image mode. The red and yellow colours correspond to gap modes (no data acquired). The major problems came from the orbit segments between Australia and Antarctic and between Africa and Antarctic where a lot of data are not acquired. This problem is under investigation by ESRIN and a new mission operation plan for the scatterometer shall be adopted.

For cycle 53 the percentage of the ERS-2 AMI activity is shown in table 7.

Table 7: ERS-2 AMI activity (cycle 53)

AMI modes	ascending passes	descending passes
Wind and Wind-Wave	**90.7%**	**84.7%**
Image	**2.2%**	**6.1%**
Gap and others	**7.1%**	**9.2%**

The percentage of scatterometer activity during the cycle 53 was within the nominal value.

Table 8 reports the major data lost due to the test periods and AMI or satellite anomalies occurred after August 6th, 1996 (before that day for many times data were not acquired due to the DC converter failure).

Table 8: ERS-2 Scatterometer mission major data lost after 6th, August 1996

From	To	Reason
September 23rd, 1996	September 26th, 1996	ERS-2 switched off due to a test period
February 14th, 1997	February 15th, 1997	ERS-2 switched off due to a depointing anomaly
June 3rd, 1998	June 6th, 1998	ERS-2 switched off due to a depointing anomaly
November 17th, 1998	November 18th, 1998	ERS-2 switched off to face out Leonide meteo storm
September 22nd 1999	September 23rd 1999	ERS-2 switched off due to Year 2000 certification test
November 17th, 1999	November 18th, 1999	ERS-2 switched off to face out Leonide meteo storm
December 31st,1999	January 2nd, 2000	ERS-2 switched off Y2K transition operation
February 7th,2000	February 9th, 2000	ERS-2 switched off due to new AOCS s/w up-link

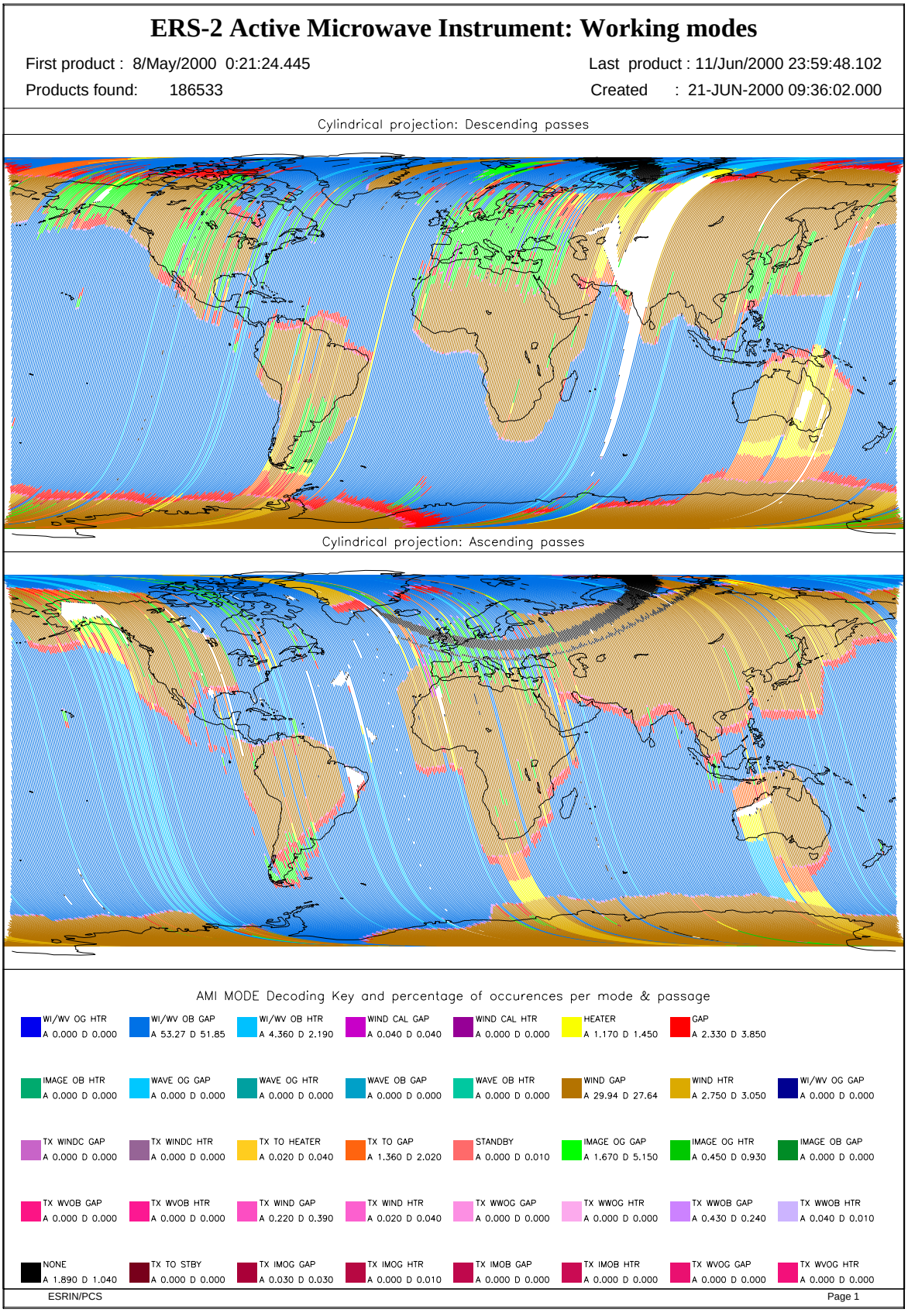

FIGURE 32. ERS-2 AMI activity during cycle 53.

The PCS carries out a quality control of the winds generated from the WSCATT data. The activity is split in two main areas: the first one includes a routine analysis of the fast Delivery Products disseminated to the users, the second one is focused on the improvement of the CMOD-4 (the operative ESA wind retrieval algorithm) for high wind speed (for more information see on the Web site http://pcswww.esrin.esa.it the Cyclone Tracking home page). External contributions to this quality control come also from ECMWF and UK-Met Office.

The routine analysis is summarized in the plots of figure 33; from top to bottom:

- the monitoring of the valid sigma-nought triplets per day.
- the evolution of the wind direction quality. The ERS wind direction (for all nodes and only for those nodes where the ambiguity removal has worked properly) is compared with the ECMWF forecast. The plot shows the percentage of nodes for which the difference falls in the range -90.0, +90.0 degrees.
- the monitoring of the percentage of nodes whose ambiguity removal works successfully.
- the comparison of the wind speed deviation: (bias and standard deviation) with the ECMWF forecast.

The results since the beginning of the mission can be summarized (after August 6th, 1996 and apart from the events given in Table 8) as:

- a stable number of valid sigma-nought with a small increase after June 29th, 1999 due to the dissemination in fast delivery of the data acquired in the Prince Albert station.
- an accurate wind direction for roughly 93% of the nodes, a success in the ambiguity removal for more than 90.0% of the nodes.

The ERS-2 wind speed shows an absolute bias of roughly 0.5 m/s and a standard deviation that ranges from 2.5 m/s to 3.5 m/s with respect to the ECMWF forecast. The wind speed bias and its standard deviation have a seasonal pattern due to the different winds distribution between the winter and summer season.

It is important to note that only after the end of calibration phase (mid March 1996) the wind products have reached high quality.

Two important changes affect the speed bias plot: the first is on June 3rd, 1996 and it is due to the switch from ERS-1 to ERS-2 data assimilation in the meteorological model. The second change, which occurred at the beginning of September 1997, is due to the new monitoring and assimilation scheme in ECMWF algorithms (4D-Var).

Since 19th April 1999 two set of meteo-table (meteorological forecast centred at 00:00 and 12:00 of each day) are used in the ground processing. With this new strategy the data are processed using the 18 and 24 hours meteorological forecast instead of the 18, 24, 30 36 hours forecast. The data processed with the 18-24 hours tables instead of 30-36 hours tables have an increase in the number of ambiguity removed nodes but no important improvements are shown, on average, in the daily statistics.

Since 25th August 1999 a new LRDPF software (version 8500) is operative in the ground stations. With this upgrade the LRDPF is year 2000 compatible; no changes were introduced in the scatterometer data processing.

The new AOCS configuration (see report for cycle 50) that is operative since 7th February 2000, did not affect the wind data performance.

For cycle 53 the PCS quality control has reported stable results.

The number of valid triplets acquired per day was stable around 180000.

The wind speed bias (UWI -ECMWF Forecast) was close to 0.1 m/s and the wind speed standard deviation was between 2.5 m/s and 3.0 m/s. The ambiguity removal rate was working fine for more than 90% of nodes.

The bad performance (high wind speed bias and low percentage of ambiguity removal rate) in the geophysical validation on 30th May 2000 is due to the spacecraft attitude. On that day the satellite was in FPM mode that is less accurate than the nominal one (YSM).

The ECMWF reports (cycle 53) an average wind speed bias of -0.78 m/s (UWI) and of -0.51 m/s (4D-Var). The wind directional bias is close to zero (both UWI and 4D-Var products) and the direction standard deviations were ranging between 30 and 65 degrees (UWI) and between 15 and 30 degrees (4D-Var). These results are comparable to the results from the previous cycle.

.

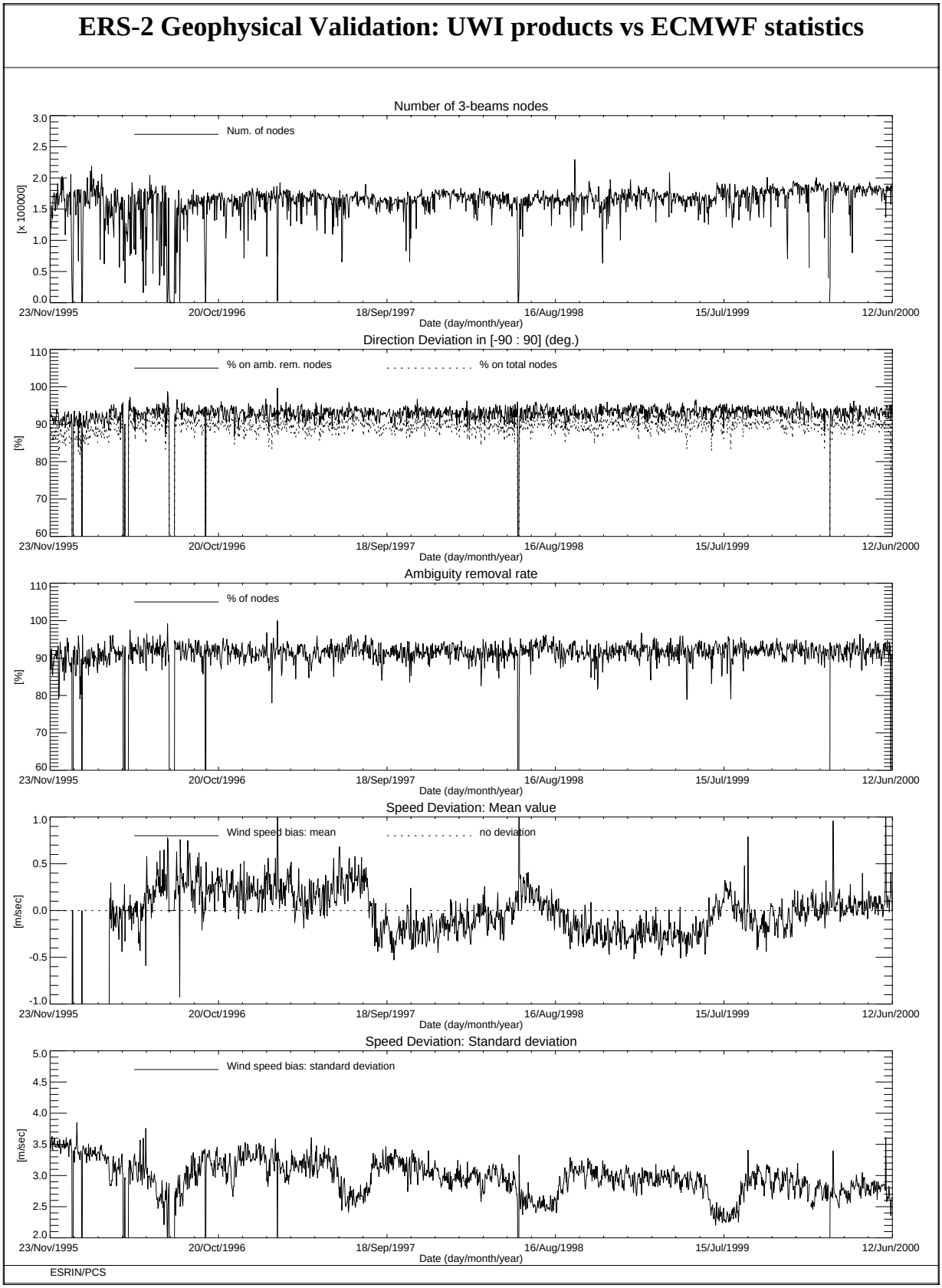

FIGURE 33. ERS-2 Scatterometer: wind products performance since the beginning of the mission.